2020

Wearable Antennas Backed by Artificial Magnetic Conductor for Enhanced Gain and Reduced Back Radiation

Steven Jacobson
smj3370@rit.edu

Wearable Antennas Backed by Artificial Magnetic Conductor for Enhanced Gain and Reduced Back Radiation

by

Steven Jacobson

Thesis Submitted

in

Partial Fulfillment of the

Requirements for the Degree of

MASTER OF SCIENCE IN ELECTRICAL ENGINEERING

Approved by:

Professor _____
Dr. Jayanti Venkataraman – Advisor

Professor _____
Dr. Panos Markopoulos – Committee Member

Professor _____
Dr. Gill Tsouri – Committee Member

Professor _____
Dr. Sohail Dianat – Department Head

DEPARTMENT OF ELECTRICAL AND MICROELECTRONIC ENGINEERING
KATE GLEASON COLLEGE OF ENGINEERING
ROCHESTER INSTITUTE OF TECHNOLOGY
ROCHESTER, NEW YORK

Acknowledgments

This work was supported by TTM Technologies, Syracuse, NY (Previously, Anaren)

I would like to thank my advisor, Dr. Jayanti Venkataraman, for her continued support, mentorship and advice during my graduate work at RIT. Her guidance and motivation in Electrical Engineering to make a real difference has been inspirational and instrumental in helping me get to this point.

I secondly need to thank my Family and Friends. Their continuous love and support helped me through this challenging journey at RIT.

Abstract

A Wireless Body Area Network (WBAN) is a system of wireless sensors and devices attached to a person's body for continuous monitoring of physiological data. These measurements can be used for a variety of purposes such as fitness tracking, personal health management or as medical diagnostic tools. In many cases, WBANs need to communicate with an off-body device to send information to healthcare providers. Wireless Medical Telemetry provides numerous benefits but has a few challenges that need to be overcome. One of the key components in this system is the antenna, which is worn on the body and typically has a broadside pattern directed out. Additionally, flexibility and miniaturization of antennas is crucial for making a comfortable and wearable antenna. Finally, the back radiation must be minimal since the dielectric properties of the human body can significantly affect the return loss, which in turn reduces the gain and distorts the radiation pattern.

The motivation of the present work is based on the need for improving the antenna, for its size, enhanced gain, with small to no back lobe and additionally on a flexible substrate to ensure patient comfort. In the present work, two antennas, a Slotted Dipole Antenna and Inverted-F Antenna have been designed at $2.5GHz$ in the Unlicensed Industrial, Scientific and Medical band (ISM). The design and modeling have been done using ANSYS HFSS (High Frequency System Simulator). A Rectangular Patch Artificial Magnetic Conductor (AMC) which is a frequency selective surface has been designed and optimized. Both antennas are backed by this AMC layer to reduce backward radiation and enhance forward gain for off body radiation.

The antennas were fabricated and validated by measurement. Both are on Rogers RT/duroid 5880 substrate ($\epsilon_r = 2.2$, $\tan\delta = 0.0009$ and dielectric height $h = 31mils$). The Inverted-F Antenna is significantly smaller than the Slotted Dipole Antenna but has a much lower

radiation gain on its own. When the antennas are integrated with the Rectangular Patch AMC their forward gains are very similar. However, the Inverted-F Antenna and AMC has a much larger front to back ratio than the Slotted Dipole Antenna and AMC. The Slotted Dipole Antenna is shown to be flexible, both concave and convex curvature are simulated. In HFSS, the effects of the human body are simulated using the Human Body Model. A SAR analysis is also performed to show the AMC layer not only directs the beam in the desired direction but reduces the amount of power absorbed by the human body significantly. The measured return loss and radiation patterns agree well with simulated results. Lastly, this work proposes an AMC unit cell that is significantly smaller than the Rectangular Patch unit cell, which has the potential to create a smaller AMC layer.

Table of Contents

List of Figures

List of Tables

1. Introduction

1.1. Biomedical Telemetry

Telemetry is best defined as data measurements being made at a distance. Telemetry systems have been used in numerous applications where testing of moving objects is required. Biomedical Telemetry is the measurement of physiological data at a distance [1]. The physiological data is collected by a medical device which can be placed on or next to a patient's body. The device can then further transmit the data to distant physicians through different communication networks. This is done in both wired and wireless schemes. Advancements in this area allow for more thorough physiological measurements of patients which could reduce complications and / or catch otherwise missed critical information. An additional advantage on top of more information but information in a timely manner.

Figure 1-1: RaceCapture/Pro3 Racecar Telemetry Device by Autosport Labs [2]

Telemetry is used in so many ways, people may not even be aware that it is happening. In Moto-sports, race car data can be sent to pit crews on the condition of the racecar with a device made by Autosport Labs, the RaceCapture/Pro3 device [2]. In the agriculture industry, soil sample measurements in the field can be taken while the information is sent back to the farmer's office

for analysis. The farmer does not need to physically be in the field to take measurements. In smart cities, Air Quality measurements and traffic conditions can be monitored and sent to a singular point. The most obvious place telemetry is used is the space industry. When sensors on satellites or space probes are sent out, telemetry is used to send the information measured back to earth for analysis [3].

Physiological Measurement devices are becoming very common. Smart Watches can measure someone's heart-rate, count their number of steps and determine if they're currently active or resting, (walking, running, sitting or sleeping). The physiological measurements can be used for numerous applications; for example, heart rate measurements, a common measurement taken by smart watches / fitness trackers, can be used for Emotion Recognition [4]. As sensor technology improves, more applications and advantages will be discovered which motivate the need for medical telemetry.

Electrocardiogram (ECG) signals can be used for accurate heart rate measurements that can lead to determining the heart's health. With more sensitive sensors than a smart watch, the ECGs can be measured and used for heart attack detection [5]. Heart Attack treatment response is critical when experiencing a cardiac event. Typically, a person would not seek medical attention until hours after experiencing symptoms; therefore, an accurate and easy way to measure this physiological data could prove to be lifesaving [5]. Welch Allyn developed a wearable sensor called the TAGecg® Wearable ECG Sensor [6]. The sensor is designed to take measurements for up to a week, after a week, the device is brought back to the physician and the data is recovered from the device and analyzed. Heart conditions that are difficult to diagnose because the symptoms are intermittent like Arrhythmias are more easily caught with continuous measurement devices like the TAGecg® Sensor.

Continuous Blood Glucose Monitors are used by many people who suffer from Diabetes. A device by Dexcom, can measure a person's blood glucose level every 5 minutes and send the data to a smart device like a smart phone [7]. This data helps people better regulate their blood sugar. It can be life saving for people who are at risk for hypoglycemia or have hypoglycemia unawareness; the system by Dexcom sends alerts to the person wearing the device and even loved ones if set up [7]. The continuously monitored data could be sent to a physician if medical attention is required. Additional physiological measurements can be taken not discussed here through wearable sensors like Blood Pressure, Blood Oxygen Saturation and Respiration [8].

(a) (b)

Figure 1-2: (a) Welch Allyn TAGecg® Sensor; (b) Dexcom Continuous Blood Glucose Meter

1.2. Wireless Body Area Networks

Wireless Medical Telemetry gives a major advantage to the medical telemetry field. Wireless Body Area Networks (WBANs) are a network of "low-power, micro and nano-technology sensors and actuators, which can be placed on the body, or implanted in the human body" [9]. WBANs allow for patients who require physiological sensors to be more mobile and active without wired devices either next to them or attached to them. In turn, the patient is given more mobility and flexibility. In addition, physicians will be able to get critical physiological measurements in a patient's 'natural' environment [9]. Wearable Wireless Body Area Networks can measure

numerous physiological qualities. Some of the applications of the measurements are used for sleep staging, Asthma / Allergic Reaction Detection, Diabetes Control, Cardiovascular Diseases and Cancer Detection [9]. In addition to multiple sensors, health monitoring on a person's smart phone can be accomplished using WBANs. [5] uses an ECG Monitor and a WBAN which connects wirelessly to a smartphone for Heart Attack detection. A typical Wireless Body Area Network can be seen in the figure below.

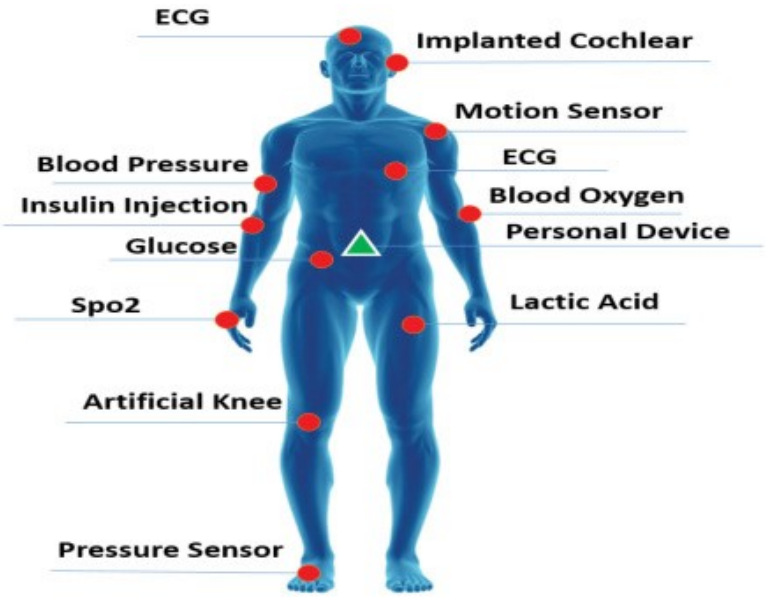

Figure 1-3: Typical Wireless Body Area Network [10]

1.2.1. Medical Frequency Bands

The Federal Communications Commission (FCC) allocates frequency bands of the electromagnetic spectrum for specific uses. In this way, frequency bands for different applications would not interfere if they were in the same proximity. Frequency bands have been allocated by the FCC for medical uses. The bands are listed in the following table with a description of what each band is typically used for.

Table 1-1: Medical Frequencies Allocated by the Federal Communications Commission (FCC) [11]

	Frequency Band	**Description**
Medical Radio Communication (MedRadio)	$401 - 406\ MHz$ $410 - 460\ MHz$	Medical devices transmitting therapeutic or diagnostic information to physicals from implanted or body-worn devices
Wireless Medical Telemetry Services (WMTS)	$608 - 614\ MHz$ $1395 - 1400\ MHz$ $1427 - 1431.5\ MHz$	Communication of Physiological Data specifically for medical uses in a hospital or physician office setting.
Medical Micro Power Networks (MMNs)	$413 - 419\ MHz$ $426 - 432\ MHz$ $432 - 444\ MHz$ $451 - 4457\ MHz$	A network of implanted and body-worn transmitters or receivers to aid in transmission of nerve and muscle stimulation.
Medical Body Area Networks	$2360 - 2400\ MHz$	Frequency band specific for a network of body-worn sensors to transmit physiological data to physicians for diagnostic and therapeutic reasons
Unlicensed Industrial, Scientific and Medical (ISM)	$13.553 - 13.567\ MHz$ $26.957 - 27.283\ MHz$ $40.66 - 40.70\ MHz$ $902 - 928\ MHz$ $2400 - 2500\ MHz$ $5725 - 5875\ MHz$ $24 - 24.25\ GHz$	Bands that do not require licensing to operate within while complying with rules for safety and limiting interference.

From Table 1-1, numerous frequency bands are designated from the FCC for medical applications. In this work, the Unlicensed ISM band of 2.4 to 2.5 GHz is chosen for the designs. The benefits of this band are that licensing is not required which makes testing and future work possible. In addition, a lot of research is already being done in this band for wireless medical telemetry thus making it a good choice for this work.

1.2.2. Challenges of Wireless Communication

The human body is destructive towards wireless transmission. Antennas placed in close proximity to the human body do not radiate well compared to the antenna away from the body's presence, in free space. The large dielectric constant of biological tissue creates dielectric loading. The additional dielectric load alters the performance of the antenna. Antenna designs for biomedical applications need to be specifically designed to account for the additional dielectric load.

Different human tissue also has different electrical properties. Therefore, if an antenna were designed for a specific location on the body, and it were moved, the dielectric loading would change, also changing the performance of the antenna. Below, electrical properties for different human tissues are tabulated.

Table 1-2: Electrical Properties of Human Tissues at $2.5GHz$ [12], [13]

Tissue	**Relative Permittivity (ϵ_r)**	**Conductivity (σ)**
Skin (Dry)	37.95	1.49
Muscle	54.35	1.92
Blood	58.18	2.59
Bone	18.49	0.822

When using antennas, the amount of energy absorbed by the human body is regulated. The Specific Absorption Rate (SAR) is used to measure the amount of energy a person's body absorbs. SAR is described as the time rate that energy is absorbed per unit of mass, or the speed at which the human body absorbs electromagnetic energy. SAR can be calculated by the following equation:

$SAR = \frac{\sigma}{\rho}|E|^2$ where ρ is the tissue density $\left[\frac{kg}{m^3}\right]$ and $|E|$ is the rms electric field value [14]. The FCC provides limits on acceptable levels of SAR for different parts of the body. This measure is significant because high levels of SAR can cause human tissue to rise in temperature. This is dangerous when the body is unable to dissipate the heat. Acceptable SAR levels are tabulated below.

Table 1-3: SAR Limits from the Federal Communications Commission (FCC) [15], [16]

SAR ($100kHz - 6GHz$)	**Whole Body**	**Partial Body**	**Hands, Wrists, Feet & Ankles**
Occupational/Controlled Exposure Limits $\left(\frac{W}{kg}\right)$	0.4	8.0	20.0
General Population/Uncontrolled Exposure Limits $\left(\frac{W}{kg}\right)$	0.08	1.6	4.0

The SAR limits in the previous table show that a person's Hands, Wrists, Feet or Ankles can be exposed to the greatest levels of radiation according to the FCC. In this work, the proposed antenna is on a person's arm, which means the maximum average SAR level is $1.6\,W/kg$ with uncontrolled exposure times, meaning the length of exposure does not need to be limited as long as the SAR stays within the limits. If the proposed antennas were moved to the wrist, larger SAR levels would be acceptable if higher powered antennas were required. SAR levels using the Human Arm Model in HFSS are simulated when each antenna configuration is backed with the proposed Artificial Magnetic Conductors.

1.3. Artificial Magnetic Conductor / Body Interference

The human body can be considered a large, lossy dielectric. Because of this, on-body antennas need to be specifically designed to cope with the dielectric load. Additionally, power output from the antenna are limited due to SAR limitations set by the FCC for safety reasons. To cope with both the dielectric load and SAR limits, a reflector can be used to prevent backward radiation and improve forward gain. One way to do this is with a perfect electric conductor. A second is with an Artificial Magnetic Conductor (AMC). A similar setup can also be used to radiate into the body to take physiological measurements [17], where an AMC is used to prevent radiation away from the body. The work in [17] shows that this setup prevents interference from movement outside of the body.

1.3.1. Perfect Electric Conductor

An Electric conductor can be used as a reflector. A grounded metal sheet would block all backward radiation from a radiating antenna. If the human body were behind the metal plate, the dielectric load would be eliminated and none of the radiation would reach the body, virtually eliminating the SAR restrictions.

The use of an electric reflector requires specific spacing between the reflector and the antenna. In order to have constructive interference, the reflector needs to be placed a quarter of the wavelength away from the antenna. At low frequencies, a quarter wavelength can be quite large. For example, at $2.5GHz$ the wavelength, λ, is equal to $120mm$. A quarter wavelength is $30mm$ or $3cm$. On a person's body, this can be quite large and bulky, therefore, it is desired to move the reflector closer to the antenna.

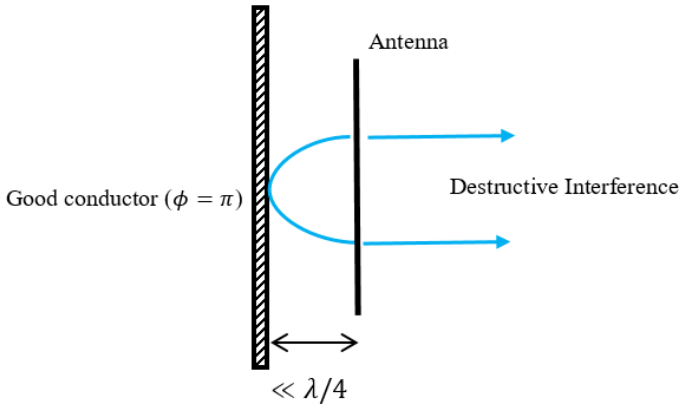

Figure 1-4: Antenna Above Electric Conductor with Spacing Less Than Quarter Wavelength [17]

The previous figure demonstrates destructive interference when an antenna is radiating too close to the good conductor because the reflected wave is out of phase with the incident wave. The next figure shows how an antenna placed a quarter wavelength away has constructive interference because the reflected wave is in phase with the incident wave.

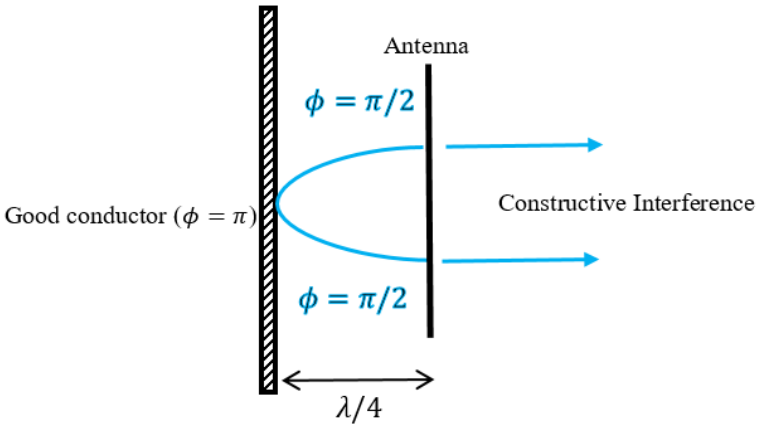

Figure 1-5: Antenna Above Electric Conductor with Spacing Equal to a Quarter Wavelength [17]

With the good conductor placed at a distance of $\lambda/4$, the total phase difference results in a reflected wave which is in phase with the incident wave, thus creating constructive interference

while blocking back radiation past the good conductor. As mentioned previously, for on-body applications, a quarter wavelength can be too bulky to wear. Investigation for methods of shrinking the spacing between a reflector and antenna is desired. A lot of work has been done using conducting sheets to remove the effects of the human body. [18] has several antennas using electric conducting sheets to block the radiation but all antenna setups are at least $5mm$ in overall height because of the required $\lambda/4$ spacing.

1.3.2. Artificial Magnetic Conductor

An Artificial Magnetic Conductor (AMC) is desired to solve the spacing issue mentioned in the previous section. With an AMC, the distance between the reflector and antenna can be reduced significantly. AMCs use the physical dimensions of the reflector to create a surface where the reflection coefficient can be modified at different frequencies based on the design. AMCs are also known as Frequency Selective Surfaces (FSS).

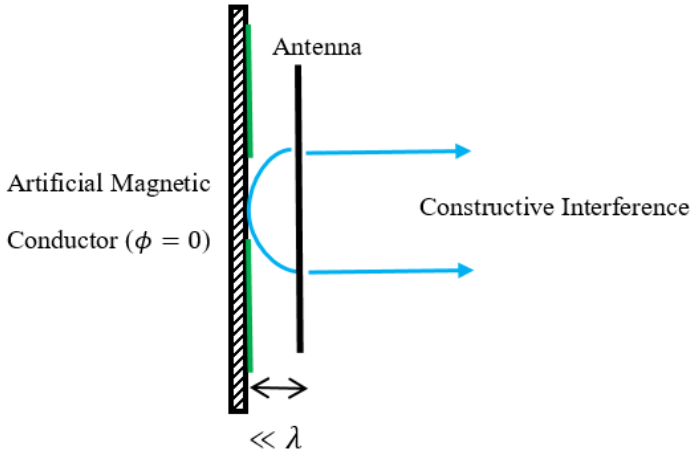

Figure 1-6: Antenna Above Artificial Magnetic Conductor with Spacing Less Than $\lambda/4$ [17]

Numerous AMC designs have been developed and tested. One of the most common AMCs is the Jerusalem Cross based AMC cell. The equivalent circuit model has been developed in [19].

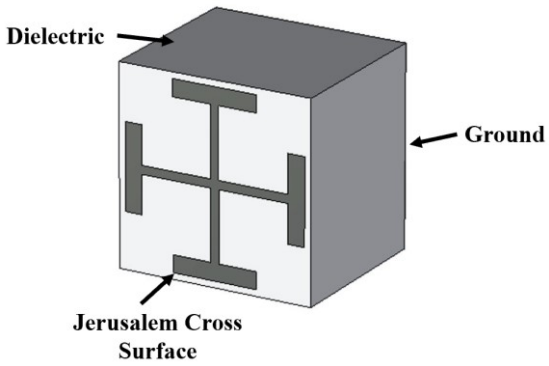

Figure 1-7: Jerusalem Cross AMC Cell Model [19]

From the work done in [19], other unit cells can be analyzed. In [17], Unit Cells like the I-Shaped, Rectangular Ring, and Rectangular Patch are further analyzed and investigated with equivalent circuit models and HFSS simulation. Each Frequency Selective Surface has its advantages and disadvantages. In order to get the reflection coefficient at the frequency desired, tuning is required. Traditional AMC cell sizes are large in relation to the operating frequency, work to miniaturize the AMC cell involves changing the design of the AMC cell itself or changing the substrate the AMC is fabricated on in order to change its effective wavelength [20].

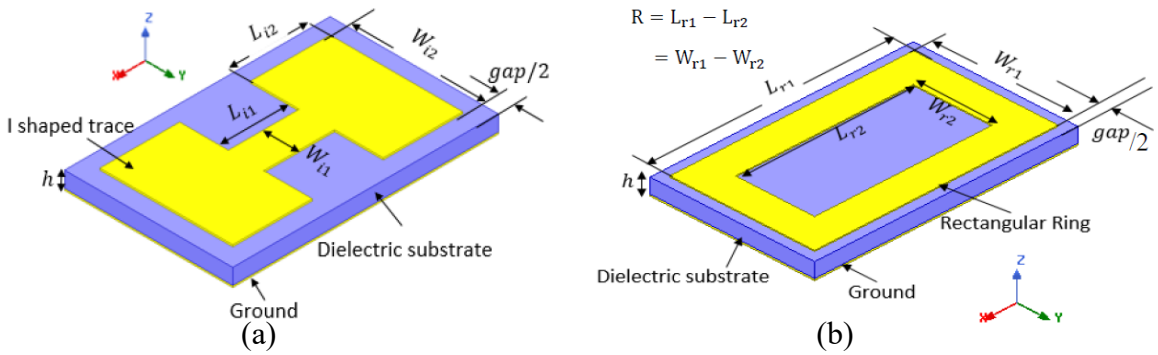

Figure 1-8: (a) I-Shaped Unit Cell; (b) Rectangular Ring Unit Cell [17]

There are many other AMC Unit Cell designs that have been investigated and tested in the literature. In this work, the Rectangular Patch AMC is investigated as well as the Square Slotted shaped AMC cell from [20]. This AMC unit cell has potential for smaller AMC layers discussed later in this thesis.

1.4. Slotted Dipole Antenna and Rectangular Patch AMC from Literature

A flexible, reconfigurable antenna backed by an Artificial Magnetic Conductor has been designed in the literature [21]. The Antenna is integrated with a PIN diode for resonance at two frequencies, $2.45GHz$ and $3.3GHz$. The Slotted Dipole Antenna is shown below.

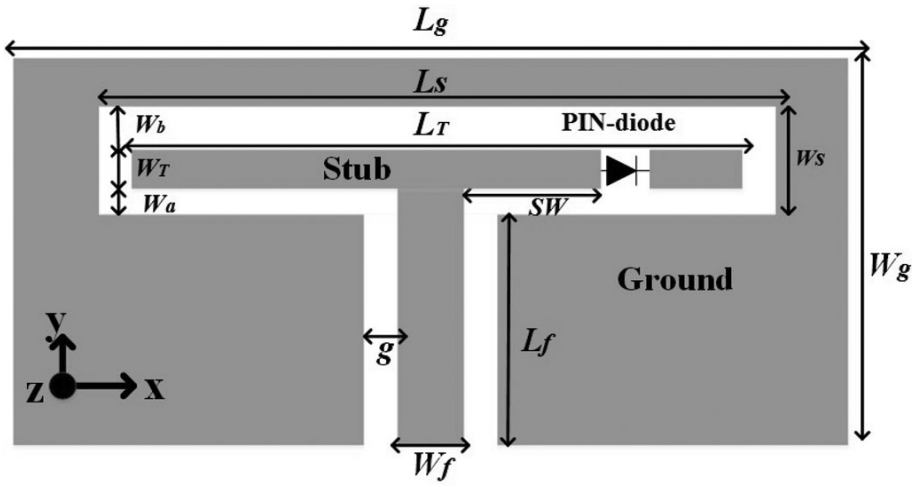

Figure 1-9: Reconfigurable Folded Slot Antenna [21]

The antenna is backed by a Rectangular Patch AMC. The AMC is also designed for two frequencies based on the polarization of the E field. By rotating the AMC 90°, the AMC can be switched between the two frequencies. The Antenna switches between the two frequencies by turning on and off the PIN diode, on for $2.45GHz$ and off for $3.3GHz$. In this work, only one frequency is required so in Section 2 the PIN diode is removed and the antenna is then optimized on a new substrate for $2.5GHz$.

Table 1-4: Slotted Dipole Antenna Dimensions [21]

Dimension	Value
L_g	$83mm$
W_g	$89mm$
L_s	$51mm$
L_T	$50mm$
W_s	$4mm$
W_a	$0.5mm$
W_b	$2.7mm$
W_T	$0.8mm$
W_f	$3.6mm$
L_f	$46mm$
g	$0.2mm$

The original substrate in [21] is Rogers RT/duroid 3003 with $\epsilon_r = 3$, $\tan\delta = 0.0013$ and dielectric height $h = 1.52mm$. The Unit Cell Design is shown in Figure 1-10

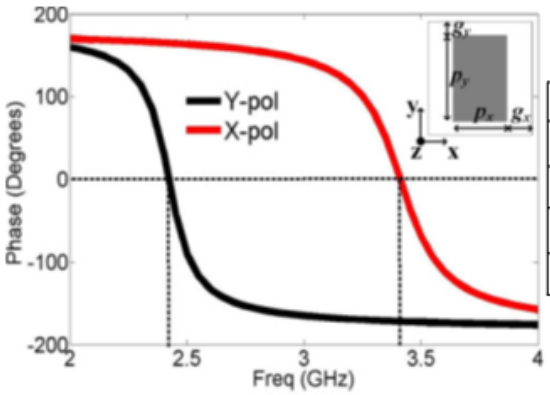

Dimension	Value
p_y	$29mm$
p_x	$23mm$
g_y	$0.5mm$
g_x	$3.0mm$

Figure 1-10: AMC Unit Cell Design [21]

The different polarization of the Unit Cell allows for use at two frequencies. The Antenna and AMC are integrated with a $6mm$ air gap and measured experimentally. The results are plotted below.

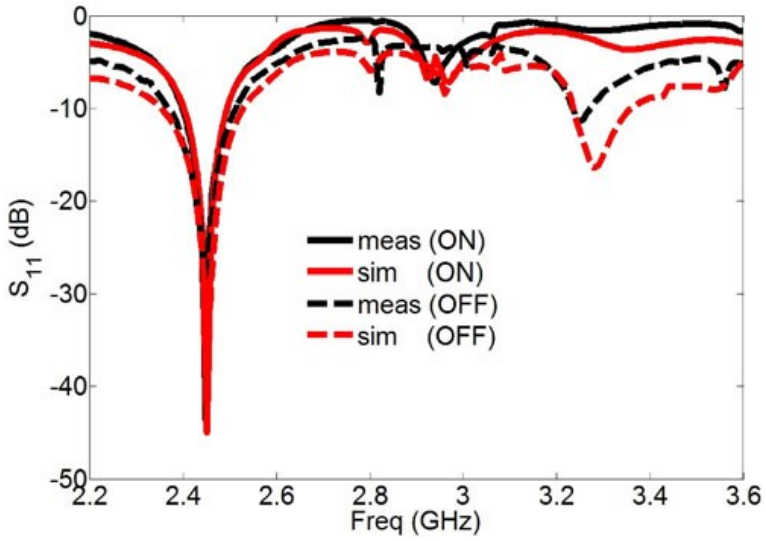

Figure 1-11: Measured and Simulated Results [21]

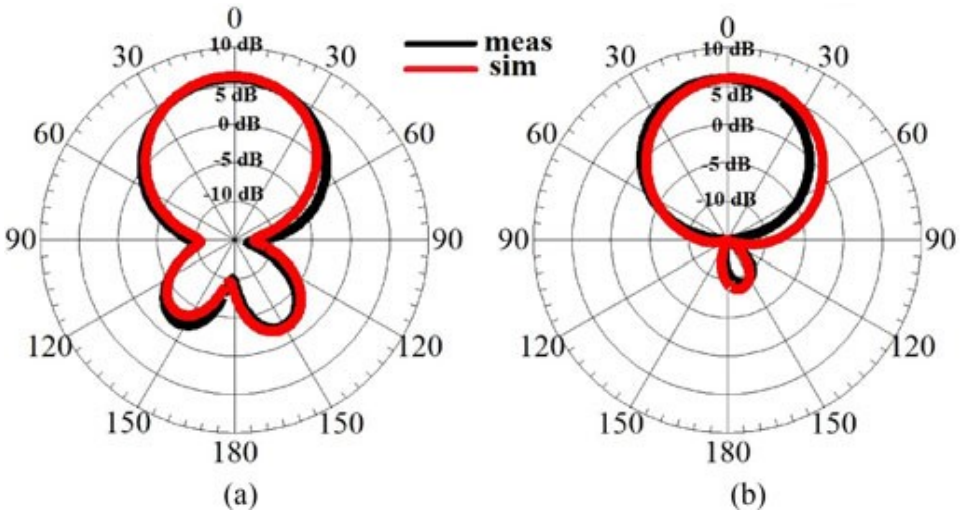

Figure 1-12: Measured and Simulated Radiation Patterns at $2.45GHz$ (diode on): (a) E-Plane; (b) H-Plane

The antenna and AMC configuration is shown to block backward radiation. The work also experimentally demonstrates flexibility of the substrate. However, the large size and large air gap makes it bulky to have as an on-body antenna.

1.5. Major Contributions of Present Work

In this work, the following contributions are made:

1) A Rectangular Patch AMC is designed at $2.5GHz$ and integrated with a Slotted Dipole Antenna. The air gap between the layers are adjusted and the antenna dimensions are adjusted for optimal electrical coupling of the two layers. Enhanced gain and front to back ratio are improved significantly with the reduced air gap configuration.
2) The Slotted Dipole and AMC are simulated on flexible substrates. Minimal changes in radiation pattern, and return loss are observed verifying the feasibility of using a flexible antenna and AMC combination.
3) An Inverted-F Antenna is designed at $2.5GHz$ and integrated with the Rectangular Patch AMC without an air gap but instead with an additional layer of substrate. A layer of substrate rather than air is ideal for an easier integration.
4) SAR simulations are performed on both the Slotted Dipole Antenna and the Inverted-F Antenna using the Human Body Model in HFSS to demonstrate the AMC layer directs the beam in the desired direction, reduces back radiation, and limits the effect of the human tissue on antenna performance.
5) A small AMC unit cell is proposed for future work. A small unit cell could allow for a small AMC layer, decreasing the overall size of the antenna AMC configuration.
6) The Antennas and Rectangular Patch AMC are fabricated on Rogers RT/duroid 5880 substrate, ($\epsilon_r = 2.2, \tan\delta = 0.0009$ and dielectric thickness $h = 31mils$). The measured results demonstrate the reduction of back radiation.

1.6. Organization of Thesis

Section 1 is an introduction to Body Area Networks and Physiological Measurements using electronic biomedical devices. A background to Artificial Magnetic Conductors is introduced with a few examples of popular Unit Cell designs and the benefits of AMC Layers of Good Conductor layers is explained.

Section 2 contains the design of a Slotted Dipole Antenna. The Antenna is backed by a Rectangular Patch Artificial Magnetic Conductor. The design of the AMC Layer is outlined as well as the critical dimensions of both the Antenna and AMC to optimize at the design frequency of $2.5GHz$. Simulations run using the Slotted Dipole Antenna with the Rectangular Patch AMC in HFSS show the reduction in back radiation and improved front to back ratio. The flexible characteristics of the Antenna and AMC are also Simulated to show the Antenna still functions as desired for more comfortable on-body applications. Additionally, the SAR directed towards the body is reduced while the effects of the human body are also eliminated.

Section 3 contains the design of an Inverted-F Antenna backed by the same Rectangular Patch AMC from Section 2. Rather than an air gap between the Inverted-F Antenna and AMC, a layer of dielectric is used. The overall height of the antenna and AMC integration is reduced and allows for easier combination. The configuration is a step towards a smaller AMC and Antenna combination by the size reduction of the Antenna.

Section 4 contains the design of a smaller AMC Unit Cell, the Square Slotted AMC Cell. The smaller cell size allows for a smaller AMC Layer. This AMC shows potential for future work with miniaturizing antenna and AMC configurations.

2. Slotted Dipole Antenna and Rectangular Patch AMC

This works' focus is the design of a flexible antenna and AMC system. An antenna in the literature is designed on Rogers RT/duroid 3003 as a Reconfigurable Slotted Dipole Antenna with an AMC Layer [21]. It is described as a wearable and flexible antenna for on-body applications where the AMC blocks back radiation towards the body. A similar design is done here on Rogers RT/duroid 5880 where the flexible capabilities are investigated in HFSS.

2.1. Slotted Dipole Antenna and AMC on Original Substrate

The Slotted Dipole Antenna and Rectangular Patch AMC from [21] was duplicated in HFSS to verify the results. The PIN diode was removed and simulated at $2.45GHz$. The antenna and AMC are designed on Rogers RT/duroid 3003, ($\epsilon_r = 3$, $\tan\delta = 0.0013$ and dielectric height $h = 1.52mm$). Table 1-4 contains the dimensions for the Slotted Dipole Antenna on this substrate and is modeled below.

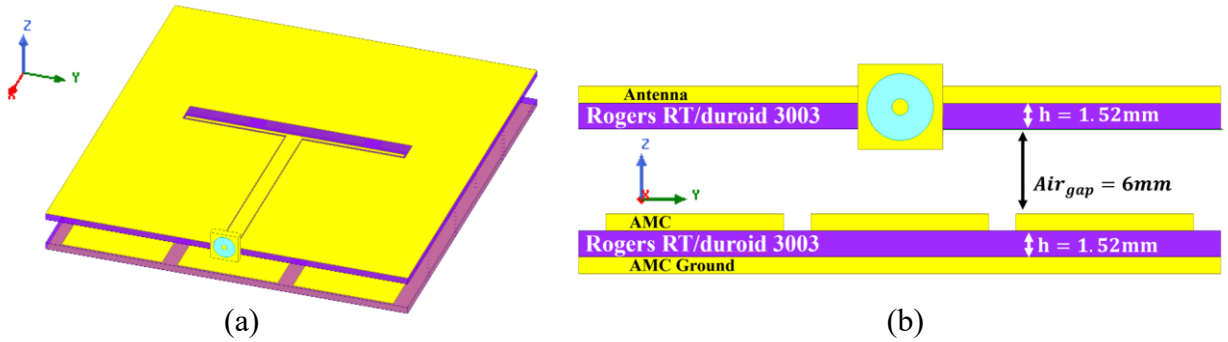

(a) (b)

Figure 2-1: HFSS Model of Slotted Dipole Antenna and Rectangular Patch AMC on Rogers RT/duroid 3003: (a) Trimetric View; (b) Cross-Section View

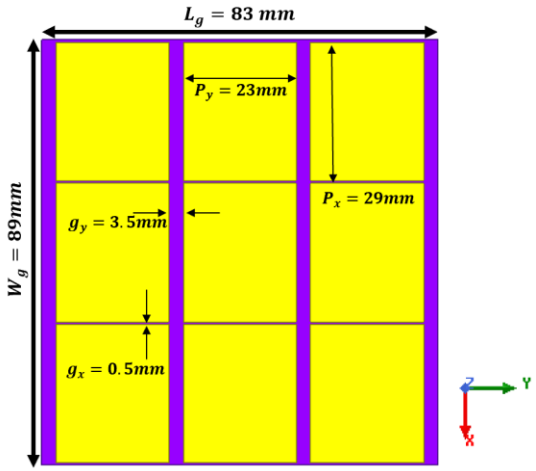

Figure 2-2: HFSS Model of Rectangular Patch AMC for $2.45GHz$ on Rogers RT/duroid 3003

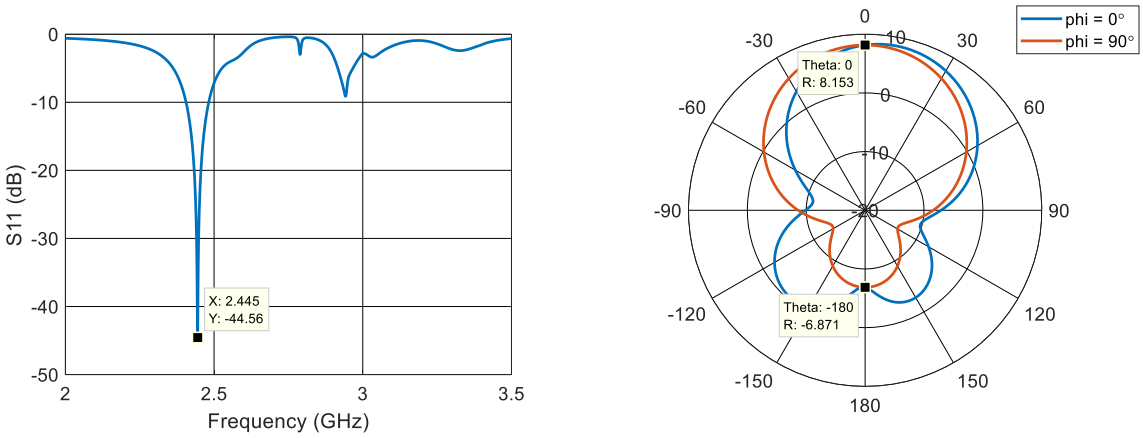

(a) (b)

Figure 2-3: Slotted Dipole Antenna with AMC on Rogers RT/duroid 3003:
(a) Return Loss; (b) Radiation Pattern

The results from this simulation match the results from [21], Figure 1-11 and Figure 1-12. This model is used as the reference for the future work in this paper. The original substrate is changed, and the Air gap is reduced in later sections. This model verifies the antenna functions without the PIN diode in place which originally made the antenna reconfigurable for two frequencies.

2.2. Slotted Dipole Antenna Optimized on New Substrate without AMC

The previous Slotted Dipole Antenna is optimized on Rogers RT/duroid 5880 ($\epsilon_r = 2.2$, $\tan\delta = 0.0009$ and dielectric height $h = 31\ mils$) from its original design in [21] and [22] to operate at $2.5GHz$. In HFSS, the design is simulated at $2.5GHz$ for its reflection coefficient and radiation pattern. The Antenna model is shown below.

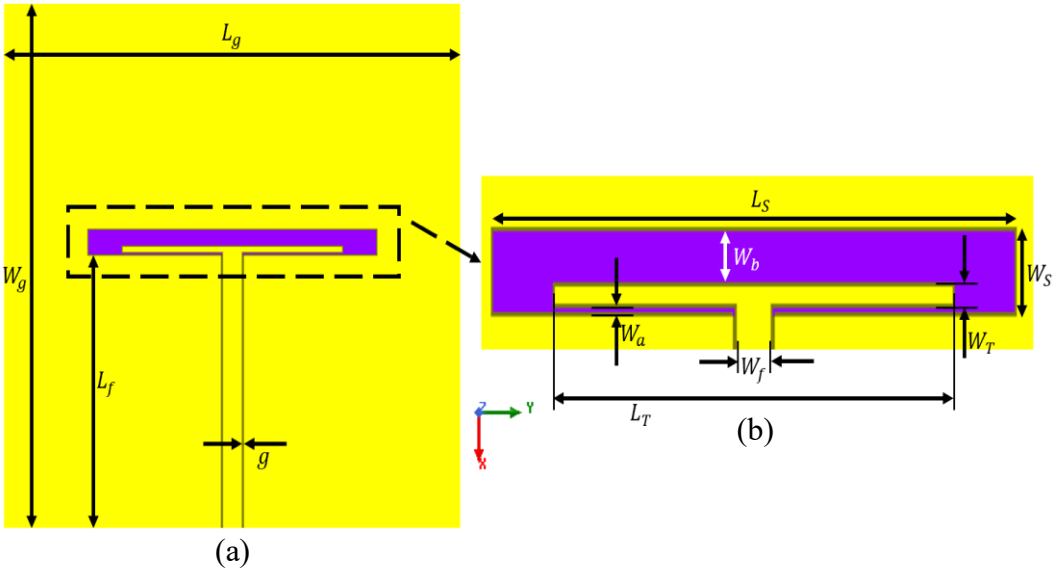

Figure 2-4: HFSS Model of Slotted Dipole Antenna without AMC Layer on Rogers RT/duroid 5880: (a) Slotted Dipole Antenna; (b) Magnified View of Slot

By adjusting critical dimensions of the antenna, the resonant frequency can be tuned for $2.5GHz$. The Antenna in [21] was on a different substrate, Rogers RT/duroid 3003 with dielectric constant $\epsilon_r = 3$ and substrate height $h = 1.52mm$. Now on the new substrate, Rogers RT/duroid 5880, two dimensions were optimized in order to change the resonant frequency, L_T, the length of the metal slot and, W_b, the width of the slot with removed copper. By adjusting L_T, the resonant frequency can be shifted while adjusting W_b, the magnitude of the return loss can be improved. The next plot shows variation in L_T and its effect on resonant frequency.

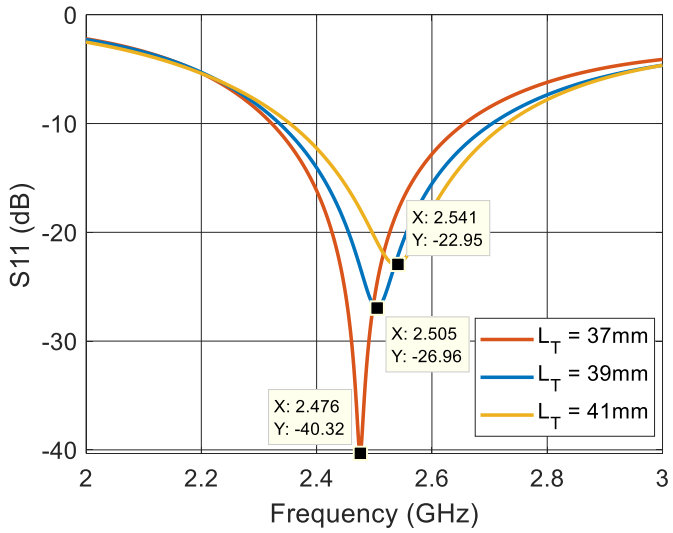

Figure 2-5: Return Loss of Slotted Dipole Antenna without AMC on Rogers RT/duroid 5880 Varying L_T ($W_b = 2.7mm$)

The different values of L_T are shown in the previous figure. As L_T increases, the resonant frequency increases as well. In addition, the return loss magnitude decreases. The desired resonant frequency is $2.5GHz$ therefore, the length of $L_T = 39mm$ is used. The next figure demonstrates what happens with the variation in W_b with the optimized L_T.

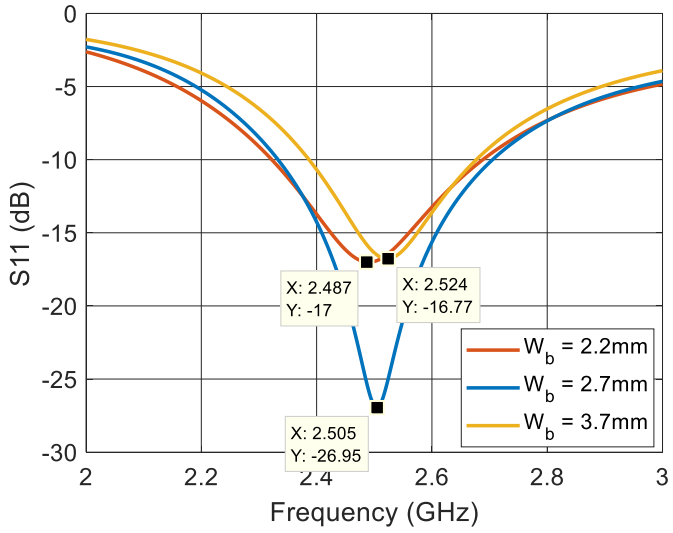

Figure 2-6: Return Loss of Slotted Dipole Antenna without AMC on Rogers RT/duroid 5880 Varying W_b ($L_T = 39mm$)

By adjusting the critical dimensions shown in Figure 2-5 and Figure 2-6, the optimal dimensions are obtained for resonance at $2.5GHz$. All the dimensions for the Slotted Dipole Antenna are shown in the following table. The optimal S11 plot of the Slotted Dipole Antenna is in Figure 2-7.

Table 2-1: Slotted Dipole Antenna Dimensions on Rogers RT/duroid 5880; $f_{resonance} = 2.5GHz$

Dimension	Value
L_g	$83mm$
W_g	$89mm$
L_s	$51mm$
L_T	$39mm$
W_s	$4mm$
W_a	$0.5mm$
W_b	$2.7mm$
W_T	$0.8mm$
W_f	$3.6mm$
L_f	$46mm$
g	$0.2mm$

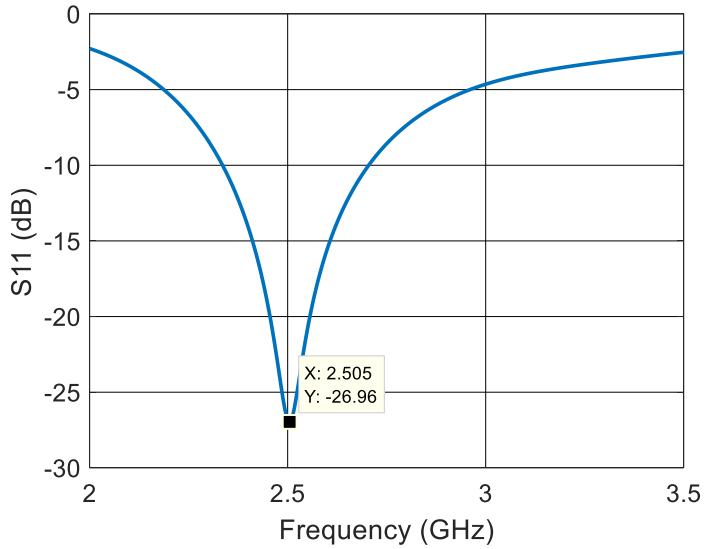

Figure 2-7: Return Loss of Slotted Dipole Antenna without AMC on Rogers RT/duroid 5880

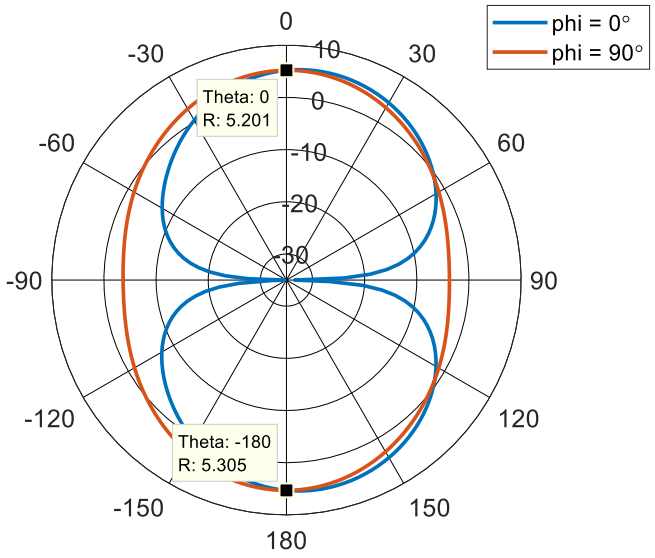

Figure 2-8: Radiation Pattern of Slotted Dipole Antenna without AMC on Rogers RT/duroid 5880

The Slotted Dipole Antenna resonates at $2.5GHz$ with return loss of $-26.96dB$. The radiation pattern shown in Figure 2-8 show radiation both above and below the antenna. It would be beneficial to block backward radiation so that the antenna becomes unidirectional. The next section designs the AMC which is then integrated with this antenna in Section 2.4.

2.3. Rectangular Patch Artificial Magnetic Conductor Optimization

The Rectangular Patch AMC from [21] is optimized at $2.5GHz$ for integration with the Slotted Dipole Antenna. The substrate for the AMC is on Rogers RT/duroid 5880 with a dielectric constant $\epsilon_r = 2.2$, $\tan\delta$ of 0.0009 and dielectric height $h = 31mils$. The optimization is done by looking at one cell from the AMC Array [17]. To keep the original dimensions of the overall AMC layer to match the dimensions of the Slotted Dipole, the dimensions of the metallic patch are adjusted while the substrate dimensions remained constant. This in turn changed the spacing between the patches as well as the sizes of the metallic patches. One dimension was found to be critical when changing the operating frequency of the AMC, p_x.

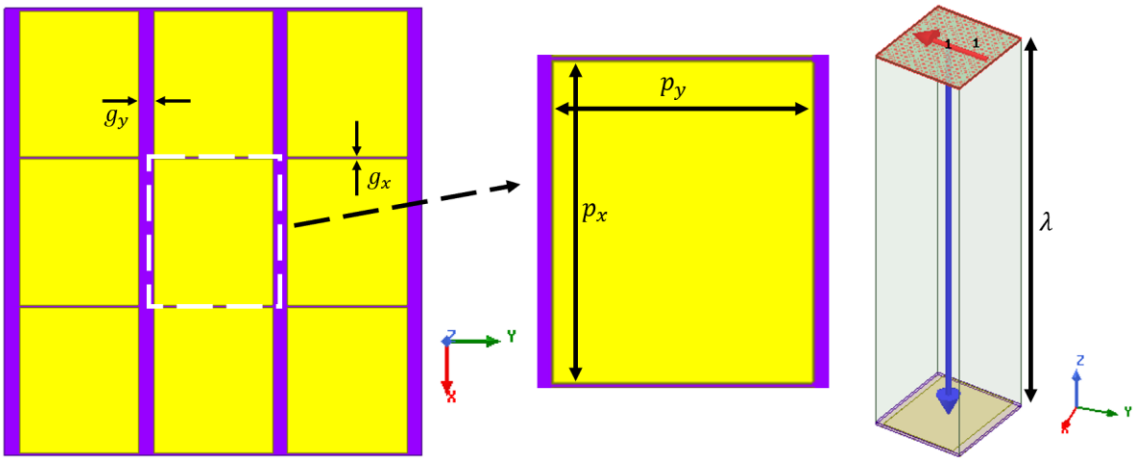

Figure 2-9: HFSS Model of AMC Unit Cell

The Unit Cell shown in Figure 2-9 is one patch or cell from the AMC array. The cell includes the metallic patch and half of the substrate spacing around the metallic patch as described in [17]. By varying p_x, the optimal dimensions of the cell were found so that there was a 0° reflection of the incident wave. The dimensions of the AMC Layer on Rogers RT/duroid 5880 are shown in Figure 2-11. The AMC can be easily optimized at other frequencies by adjusting the p_x dimension, which also changes g_x.

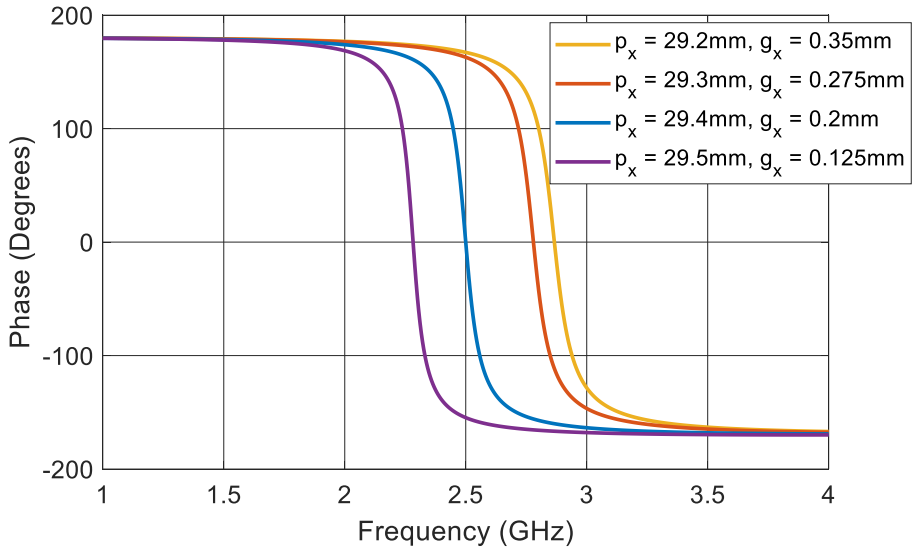

Figure 2-10: Phase Plot of Rectangular AMC Patch for Different Values of p_x, ($p_y = 23mm$)

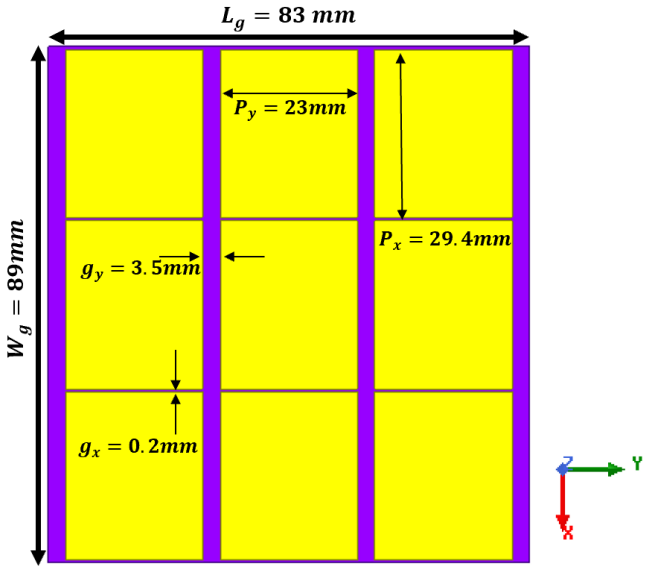

Figure 2-11: HFSS Model of Artificial Magnetic Conductor for $2.5GHz$ on Rogers RT/duroid 5880

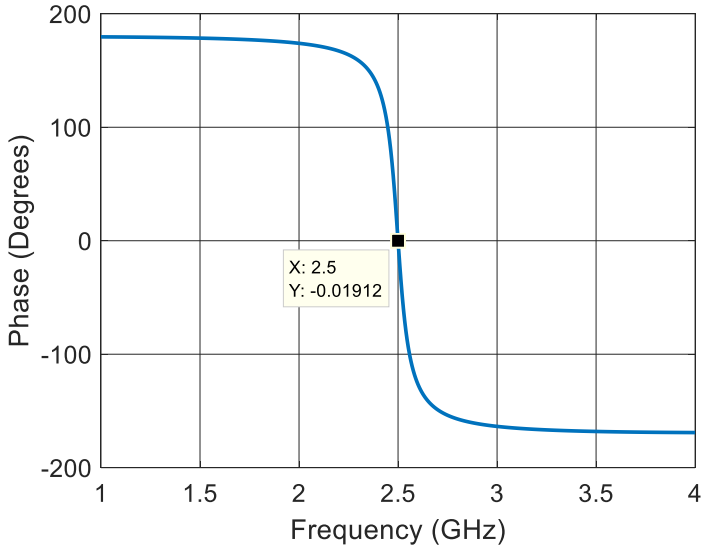

Figure 2-12: Phase Plot of Optimized Rectangular AMC Patch on Rogers RT/duroid 5880

Figure 2-12 shows that at $2.5GHz$ there is a $-0.019°$ phase difference between the incident and reflected wave. The dimensions for the AMC with this patch size are in Figure 2-11. This AMC layer is used in the coming sections for integration with the Slotted Dipole Antenna.

2.4. Slotted Dipole Antenna and Rectangular Patch AMC Integration

The antenna from Section 2.2 and AMC from Section 2.3 are put together in this section. Their integration is essential to block the backward radiation from the antenna and improve the forward gain. The configuration is incredibly sensitive to where the radiating slot is with reference to the AMC layer. Tuning is required to determine the optimal position of the slot of the antenna. By varying the length of the feedline, L_f, to move the location of the slot, the best dimensions can be found. First, the air gap of $6mm$ is optimized (Air_{gap}), the optimal feedline length is $L_f = 29mm$.

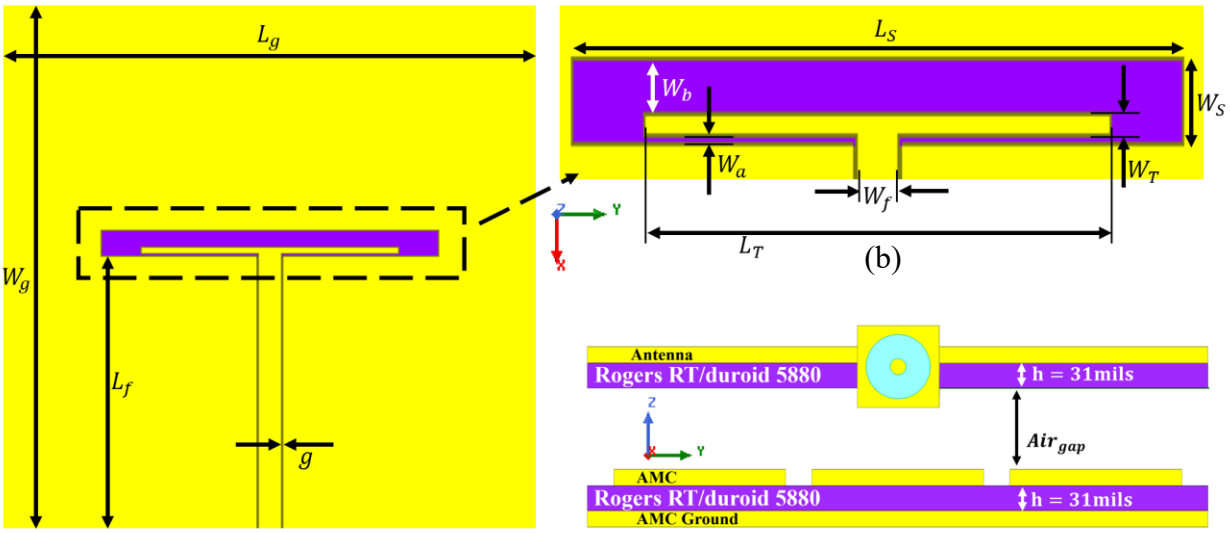

Figure 2-13: HFSS Model of Slotted Dipole Antenna with AMC:
(a) Slotted Dipole Antenna; (b) Magnified View of Slot; (c) Cross-Section View

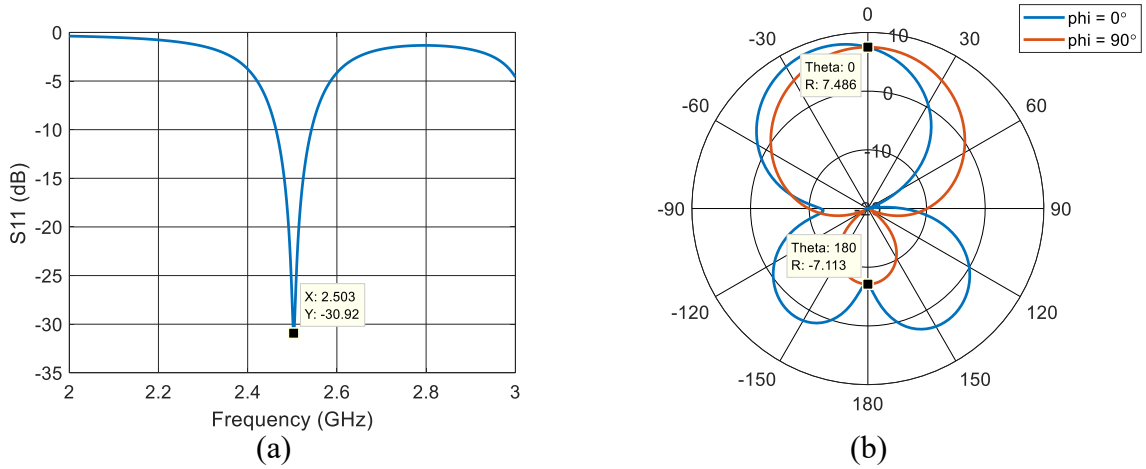

(a) (b)

Figure 2-14: Slotted Dipole Antenna with AMC on Rogers RT/duroid 5880 ($Air_{gap} = 6mm, L_f = 29mm$)
(a) Return Loss; (b) Radiation Pattern

The current configuration resonates at $2.5GHz$ with a return loss of $-30.92dB$. The antenna also has total forward gain of $7.486dB$. The back radiation is significantly reduced with this configuration and improves the forward gain in comparison with the antenna alone in Section 2.2 and Figure 2-8. The setup has a front to back ratio of $14.6dB$ but its worst-case front to back ratio of $4.2dB$. The worst-case front to back ratio is a measure of the maximum backward gain compared to the maximum forward gain. The standard front to back ratio is measured from directly forward to directly behind the antenna configuration, in other words at $0°$ and $180°$. For a lower profile configuration, the air gap was reduced to $Air_{gap} = 1mm$ and the length of the feedline was adjusted again to find the optimal dimension to be $L_f = 40mm$.

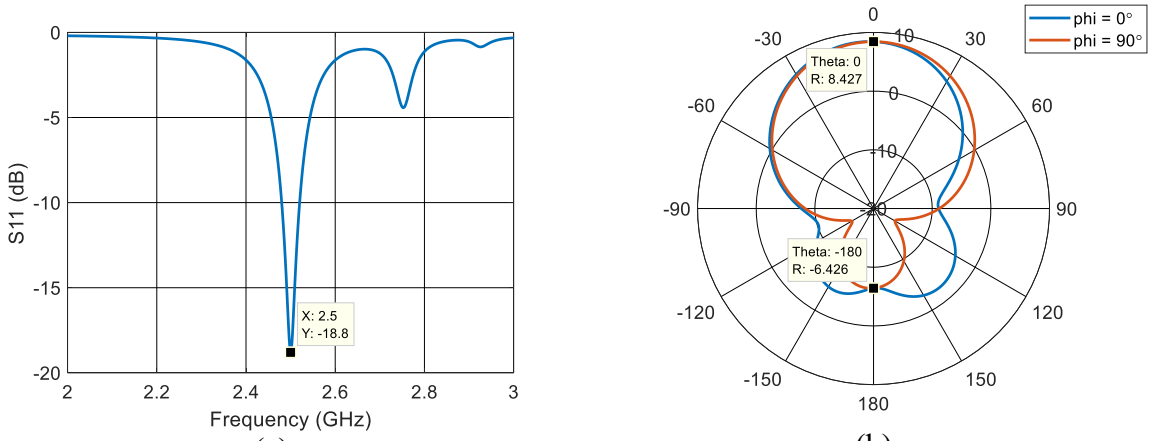

(a) (b)

Figure 2-15: Slotted Dipole Antenna with AMC on Rogers RT/duroid 5880 $(Air_{gap} = 1mm, L_f = 40mm)$
(a) Return Loss; (b) Radiation Pattern

Reducing the air gap between the Slotted Dipole Antenna and AMC layer reduced the magnitude of the return loss. The return loss is now $-18.8dB$. However, the forward gain of the antenna increased to $8.427dB$ with a front to back ratio of $14.85dB$. The worst-case front to back ratio increases significantly with this change to $10.8dB$. Table 2-2 tabulates the results of the simulations for both configurations of Slotted Dipole Antenna with the AMC layer.

Table 2-2: Results of Slotted Dipole Antenna and AMC Spacing on Rogers RT/duroid 5880 $Air_{gap} = 6mm$, and $Air_{gap} = 1mm$

	Results	
	$\boldsymbol{Air_{gap} = 6mm}$	$\boldsymbol{Air_{gap} = 1mm}$
$\boldsymbol{L_f}$	$29mm$	$40mm$
$\boldsymbol{f_{resonance}}$	$2.5GHz$	$2.5GHz$
Return Loss	$-30.92dB$	$-18.8dB$
Forward Gain	$7.486dB$	$8.427dB$
Front to Back Ratio	$14.6dB$	$14.85dB$
Worst-Case Front to Back Ratio	$4.2dB$	$10.8dB$

The air gap is reduced in this section for the optimized Slotted Dipole Antenna and Rectangular Patch AMC. In order for the Antenna to couple well with the AMC, the location of the radiating slot needed to be adjusted. This adjustment is made by changing the length of the feedline, L_f. After good coupling is acquired, the simulation results show that the smaller air gap has a higher forward gain of $8.427dB$ but about the same front to back ratio, $14.8dB$. But the worst-case front to back ratio increases significantly from $4.2dB$ to $10.8dB$. When the air gap is reduced, the AMC is blocking more back radiation than previously. In most other aspects, the two function the same once the optimal location of the radiating slot is found.

2.5. Effects of Flexible Substrate

For improved patient comfort, a flexible substrate is desired. If the setup were placed on a patient's arm or leg, the flexing abilities would allow for the antenna to contour to the patient's body. Rogers RT/duroid 5880 is flexible. Using HFSS, two curvatures are simulated to verify the functionality of curving the substrate of both the antenna and AMC.

2.5.1. Flexible Substrate with Concave Curvature

The first curvature investigated is the Concave Curvature. This setup is preferable for into-body radiation as the antenna side of the setup would be curved to contour the body. The same antenna dimensions from Section 2.4 are used for the curvature model with an air gap of $6mm$. The Antenna has a curve radius of $83mm$. With the $6mm$ air gap, the antenna is simulated in HFSS for its input impedance and radiation pattern. The simulation is performed in free space.

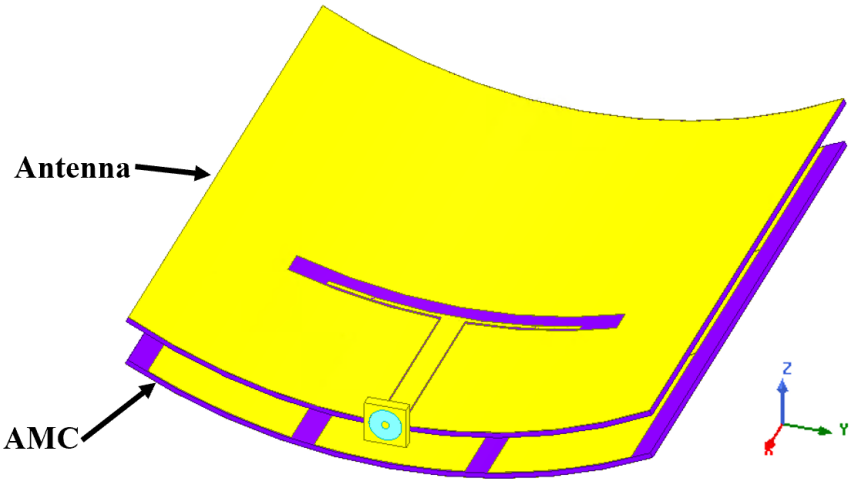

Figure 2-16: HFSS Model of Flexible Substrate with Concave Curvature of Antenna and AMC $(Air_{gap} = 6mm)$

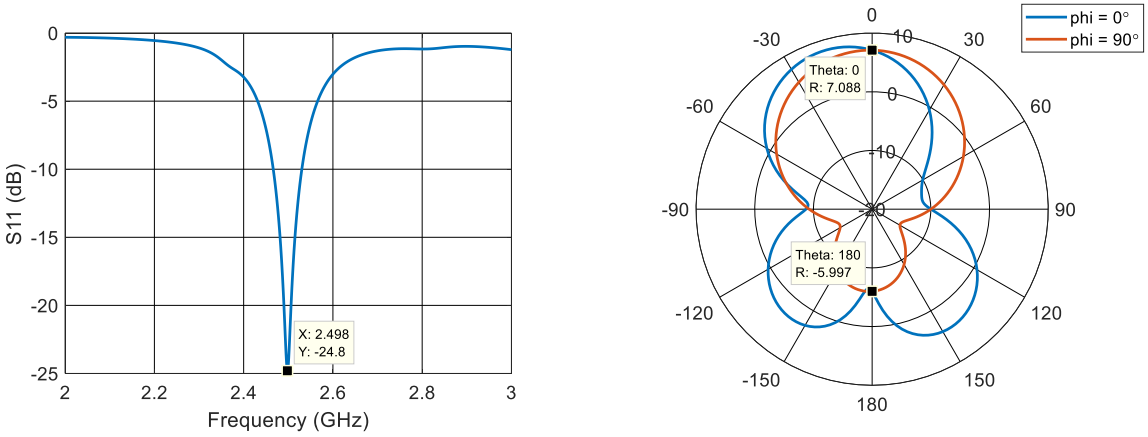

(a) (b)

Figure 2-17: Flexible Substrate with Concave Curvature: (a) Return Loss; (b) Radiation Pattern $(Air_{gap} = 6mm, L_f = 29mm)$

The Slotted Dipole Antenna with a Concave Curvature has a Return Loss of $-24.8dB$. The magnitude of the Return Loss decreased compared to the flat antenna configuration with an air gap of $6mm$, Figure 2-14. The antenna still resonates at $2.5GHz$ and the forward gain of the antenna is slightly reduced to $7.08dB$. The front to back ratio is $13.08dB$ with a worst-case front to back ratio of $3dB$. Both are slightly less than the flat Antenna and AMC configuration.

2.5.2. Flexible Substrate with Convex Curvature

The second curvature is the Convex Curvature. This setup is for off-body communication where the antenna would radiate away from the body, the AMC layer would be on the body-side of the configuration and the antenna would be on the outside. The same antenna and AMC dimensions from section 2.4 are used for the curvature model with an air gap of $6mm$. The Antenna has a curve radius of $83mm$.

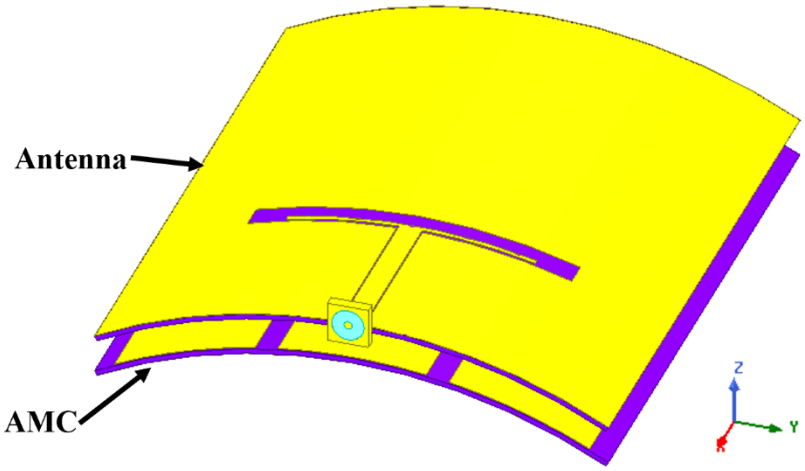

Figure 2-18: HFSS Model of Flexible Substrate with Convex Curvature of Antenna and AMC $(Air_{gap} = 6mm)$

The configuration has an air gap of $6mm$ between the Antenna and AMC layer. Both layers have the same curve radius of $83mm$. As discussed in Section 2.4, the location of the radiating slot in reference to the AMC is critical. For the $6mm$ air gap, the same feedline length of $L_f = 29mm$ is used in the Convex Curvature Model. The results of the simulation are shown in Figure 2-19. This antenna configuration resonates at $2.5GHz$ with a return loss of $-26.08dB$. The forward gain is slightly larger than the Concave Curvature at $7.11dB$.

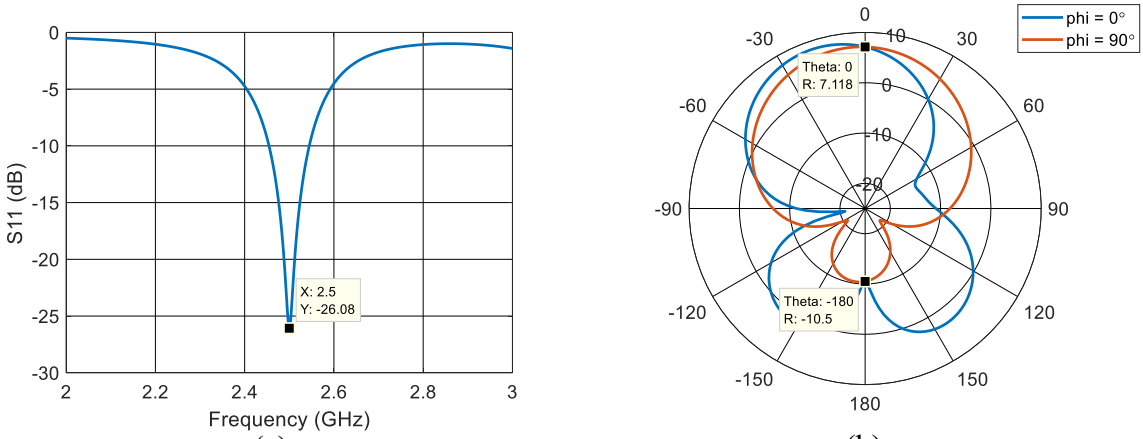

(a) (b)

Figure 2-19: Flexible Substrate with Convex Curvature: (a) Return Loss; (b) Radiation Pattern $(Air_{gap} = 6mm, L_f = 29mm)$

Table 2-3: Effects of Flexible Substrate on Slotted Dipole Antenna and AMC ($Air_{gap} = 6mm$)

	Flat	**Concave**	**Convex**
$f_{resonance}$	$2.5GHz$	$2.498GHz$	$2.5GHz$
Return Loss	$-30.92dB$	$-24.8dB$	$-26.08dB$
Forward Gain	$7.486dB$	$7.08dB$	$7.11dB$
Front to Back Ratio	$14.6dB$	$13.08dB$	$17.61dB$
Worst-Case Front to Back Ratio	$4.28dB$	$3dB$	$4.42dB$
	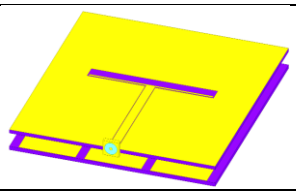	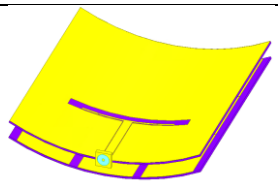	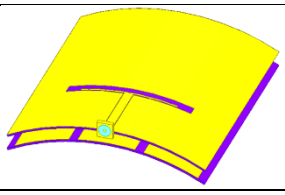

The flexible substrate is simulated with $Air_{gap} = 6mm$ for each configuration analyzed. The Convex Curvature of the Slotted Dipole Antenna with AMC performed slightly better than the Concave Curvature, but not as well as the flat configuration. The Convex Curvature has a Return Loss of $-26.08dB$ and forward gain of $7.11dB$. The Antenna has a front to back ratio of $17.61dB$. The configuration's worst-case front to back ratio is $4.42dB$. In all aspects, this configuration performed better than the Concave Curvature configuration, but not as well as the flat configuration. The performance of all the flexible antenna configurations could most likely be

improved by decreasing the air gap between the Antenna and AMC layers. Although the flat antenna configuration may have higher forward gain of $7.486dB$, the flexible substrate has little effect on the flexible antennas; therefore, a flexible substrate is feasible for the Slotted Dipole Antenna and Rectangular Patch AMC. The influence of the flexible substrate is shown in Table 2-3.

2.6. Slotted Dipole Antenna with Human Body Model without AMC Layer

The Human Body is very lossy; to demonstrate the effect this has on the antenna, the Human Body model is used in HFSS. The antenna without the AMC is placed approximately $2mm$ above the Human Arm Model shown in Figure 2-20. The Human Arm Model uses the material "Human Average" which takes an average of the body's dielectric constant for the material.

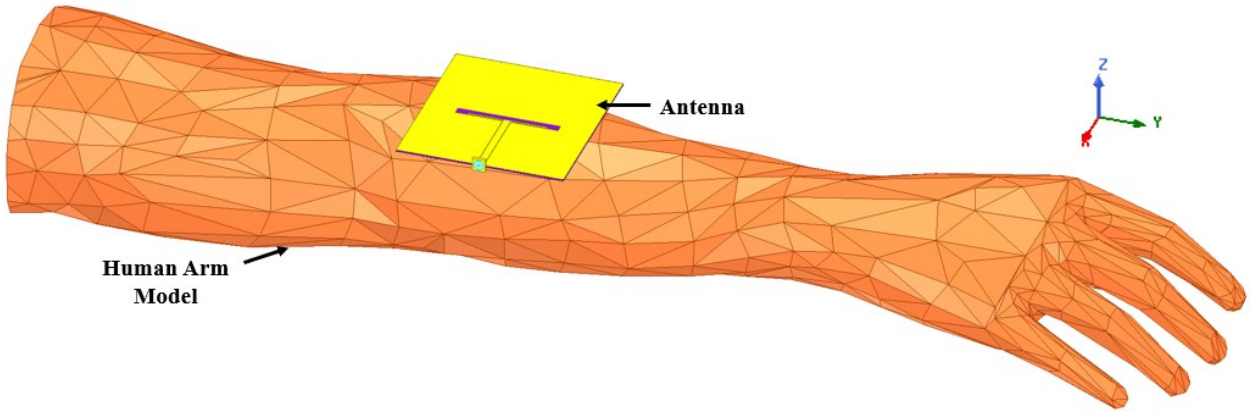

Figure 2-20: HFSS Model of Slotted Dipole Antenna without AMC above Human Arm

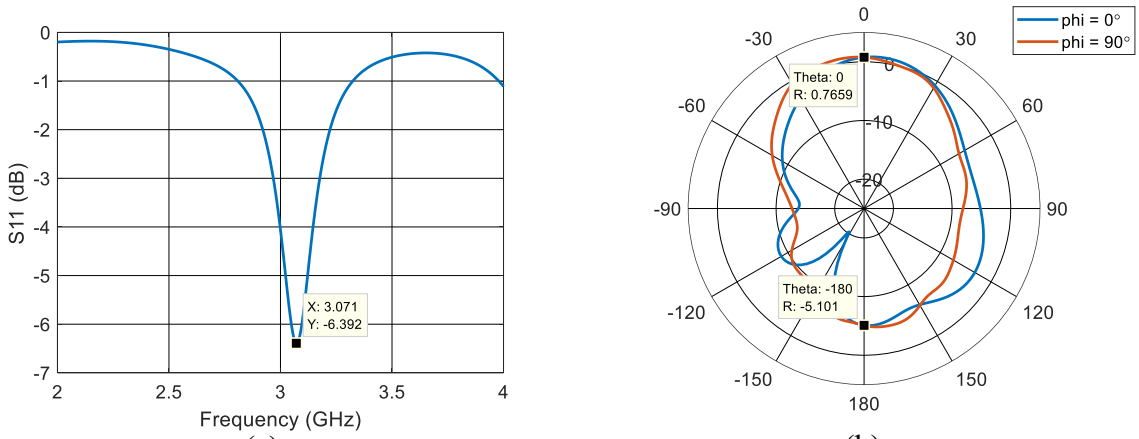

(a) (b)

Figure 2-21: Slotted Dipole Antenna without AMC placed above Human Arm: (a) Return Loss; (b) Radiation Pattern

The Slotted Dipole Antenna in free space should function as seen in Section 2.2. It was originally designed to resonate at $2.5GHz$, but once the Human Arm is introduced, the frequency shifts to $3.07GHz$ with a Return Loss of $-6.39dB$, therefore demonstrating the antenna is no longer functioning as desired. This is attributed to the dielectric load due to the human body. These results demonstrate the need for an additional layer to make the omnidirectional antenna into a unidirectional antenna and AMC combination. The average SAR imposed on the Human Arm Model is shown in Figure 2-22.

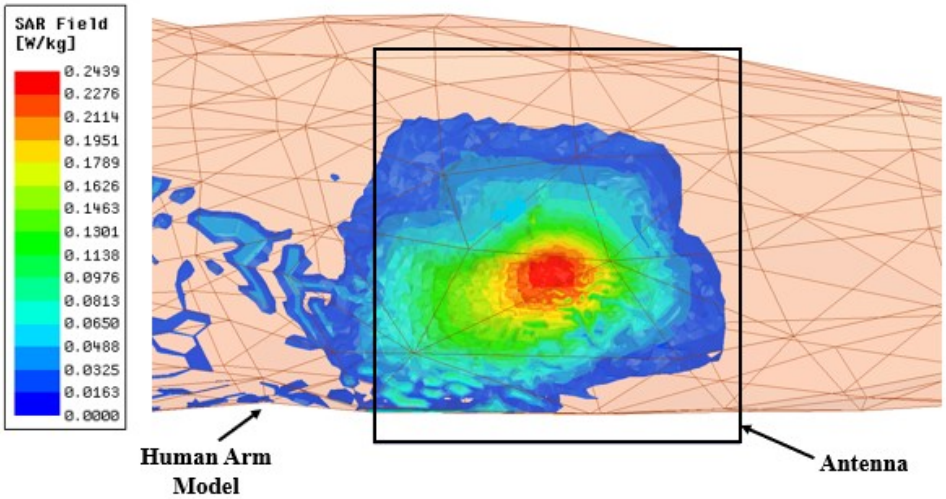

Figure 2-22: Average SAR Simulation of Slotted Dipole Antenna without AMC (Input Power: $10mW$)

The SAR simulation shows that with the Slotted Dipole Antenna, the maximum average SAR is $0.2439 W/kg$ when the AMC layer is not included. This is within the limits imposed by the FCC; however, the results of the simulation show the frequency shift rendering the antenna useless on the arm in this configuration. The next section simulates the Slotted Dipole Antenna with the AMC layer to show how the effect of the human tissue is removed.

2.7. Slotted Dipole Antenna with Human Body Model with AMC Layer

Section 2.6 shows the simulation results of the Slotted Dipole Antenna without the AMC layer on the Human Arm Model in HFSS. The antenna did not function as intended because of the large dielectric load from the human body seen in Figure 2-21. In this section, the AMC layer is added back to the Antenna Model and the Human Arm Model using Human Average material is introduced again. The human tissue should have little to no effect on the antenna performance because the AMC Layer blocks backward radiation.

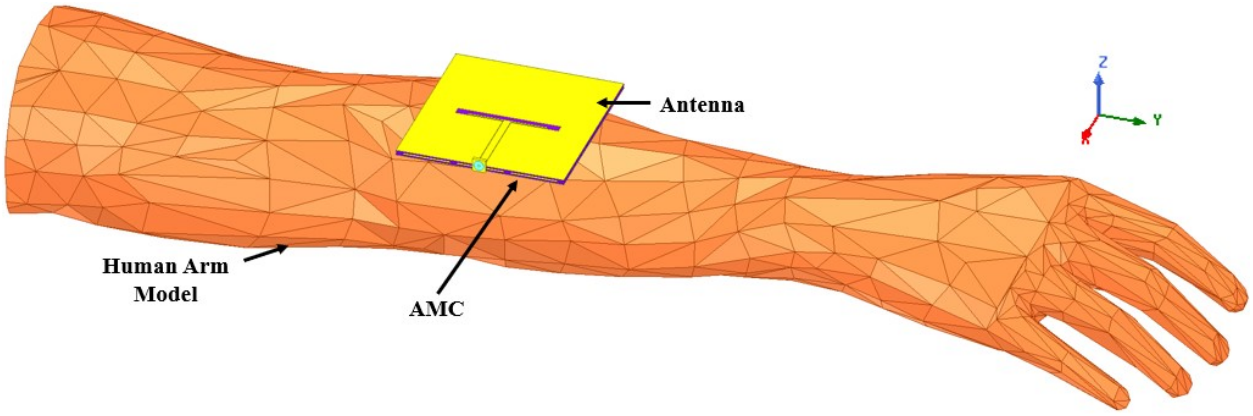

Figure 2-23: HFSS Model of Slotted Dipole Antenna with AMC above Human Arm

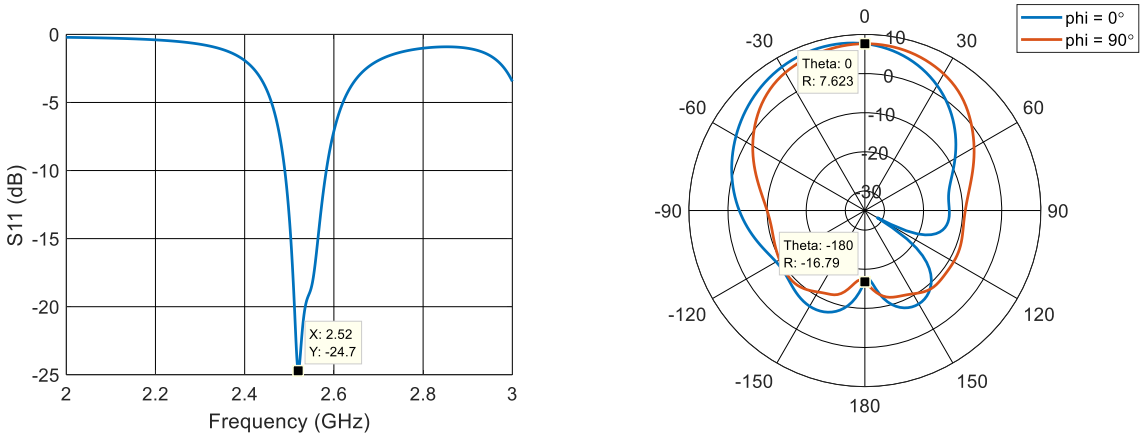

(a) (b)

Figure 2-24: Slotted Dipole Antenna with AMC Placed Above Human Arm: (a) Return Loss; (b) Radiation Pattern

The results in the previous figure show that with the AMC layer, the antenna configuration still functions as designed despite the proximity to the Human Arm Model. There is a slight shift in resonant frequency to 2.52 GHz, but the radiation pattern is still what is expected. The forward gain is $7.6dB$, which is only $0.8dB$ less than when the Human Arm is not included in the model. The SAR levels is determined through the simulation as well. In Figure 2-25, the average SAR on the human arm model is shown below. As per Table 1-3, the maximum SAR level the human arm can encounter is through controlled exposure is $1.6\ W/kg$.

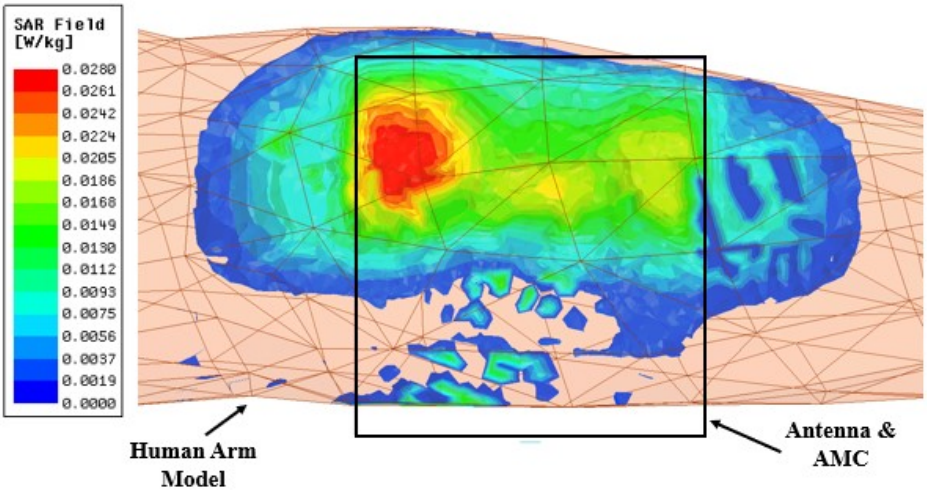

Figure 2-25: Average SAR Simulation of Slotted Dipole Antenna with AMC (Input Power: $10mW$)

The simulation shows that with the AMC layer under the Slotted Dipole Antenna, the SAR levels are still well under the limits provided by the FCC while the performance of the antenna is still preferable. The maximum average SAR level reached $0.028\,W/kg$, with input power of $10mW$ to the Slotted Dipole Antenna, far below the limit imposed by the FCC. This measurement is lower than the average SAR of the Slotted Dipole Antenna without the AMC as expected because the AMC blocks backward radiation. A comparison of the Slotted Dipole Antenna with the Rectangular Patch AMC with $Air_{gap} = 1mm$ is shown in Table 2-4 when placed on the Human Arm Model.

Table 2-4: Slotted Dipole Antenna on Arm Simulation Results $(Air_{gap} = 1mm)$

	Free Space with AMC	**Arm no AMC**	**Arm with AMC**
$f_{resonance}$	$2.5GHz$	$3.071GHz$	$2.52GHz$
Return Loss	$-18.8dB$	$-6.39dB$	$-24.7dB$
Forward Gain	$8.427dB$	$0.766dB$	$7.623dB$
SAR	–	$0.244\,W/kg$	$0.028\,W/kg$
	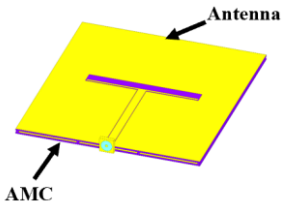	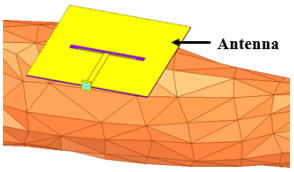	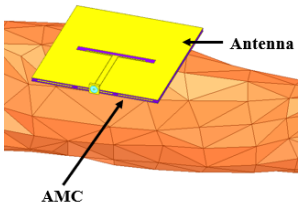

The Human Arm Model significantly effects the performance of the Slotted Dipole Antenna when the AMC layer is not included with a large shift in resonant frequency to $3.071GHz$ and very poor return loss, $-6.39dB$. With the AMC layer, the antenna functions almost as if the Human Arm Model is not included with a very slight shift in resonant frequency to $2.52GHz$ and good return loss, $-24.7dB$. In addition, the SAR level with the AMC is shown to be significantly lower at $0.028\,W/kg$, compared to when the AMC is not included, although both are within the guidelines from the FCC.

2.8. Experimental Validation

The Slotted Dipole Antenna and Rectangular Patch AMC were fabricated on Rogers RT/duroid 5880, ($\epsilon_r = 2.2, \tan\delta = 0.0009$ and $h = 31mils$), for $Air_{gap} = 1mm$ configuration. In this section, the Slotted Dipole Antenna and AMC are experimentally measured using the HP8753ET Network Analyzer and the Anechoic chamber.

2.8.1. Measured Slotted Dipole Antenna without AMC

The Slotted Dipole Antenna is experimentally tested in this section. The Network Analyzer is used to obtain the Return Loss of the Slotted Dipole Antenna in free space. The fabricated antenna dimensions are visible in Table 2-1. With the exception of $L_f = 40mm$ for the $Air_{gap} = 1mm$ configuration shown in Table 2-2.

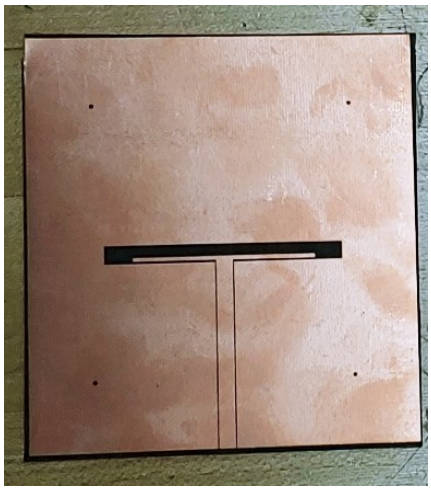

Figure 2-26: Fabricated Slotted Dipole Antenna

In Figure 2-27 the Return Loss of the fabricated antenna is plotted. The measured Slotted Dipole Antenna has a slight shift in resonant frequency from $2.505GHz$ to $2.485GHz$ after fabrication, but still has very good return loss at $-34.53dB$. Below the Radiation Pattern is plotted.

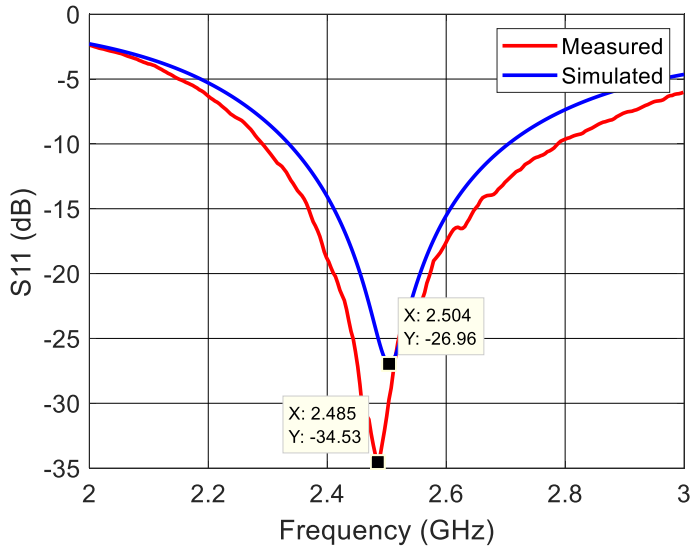

Figure 2-27: Slotted Dipole Antenna without AMC Measured and Simulated Return Loss

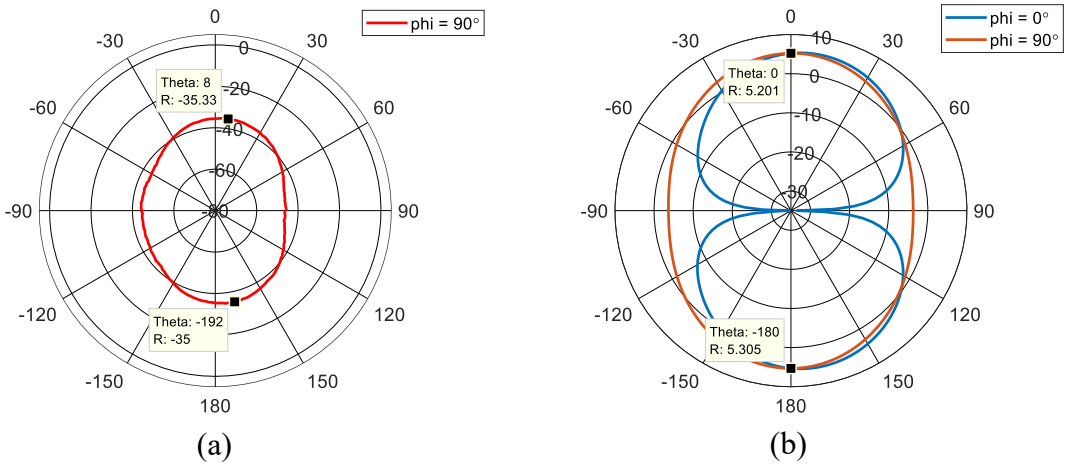

(a) (b)

Figure 2-28: Slotted Dipole Antenna without AMC Radiation Pattern:
(a) Measured (dBm); (b) Simulated

Compared with Figure 2-8, the radiation pattern is similar. The shifts in peaks of the measured results can be attributed to measurement issues with the automated system in the Anechoic chamber. The antenna is integrated with the Rectangular Patch Artificial Magnetic Conductor in the next section.

2.8.2. Measured Slotted Dipole Antenna with Rectangular Patch AMC

The Slotted Dipole Antenna and Rectangular Patch AMC are integrated using nylon screws and washers. The washers are $1mm$ in height to provide the spacing for $Air_{gap} = 1mm$. The HP8753ET Network Analyzer and Anechoic Chamber are used to measure the Return Loss and Radiation Pattern of the Slotted Dipole Antenna backed by the Rectangular Patch AMC.

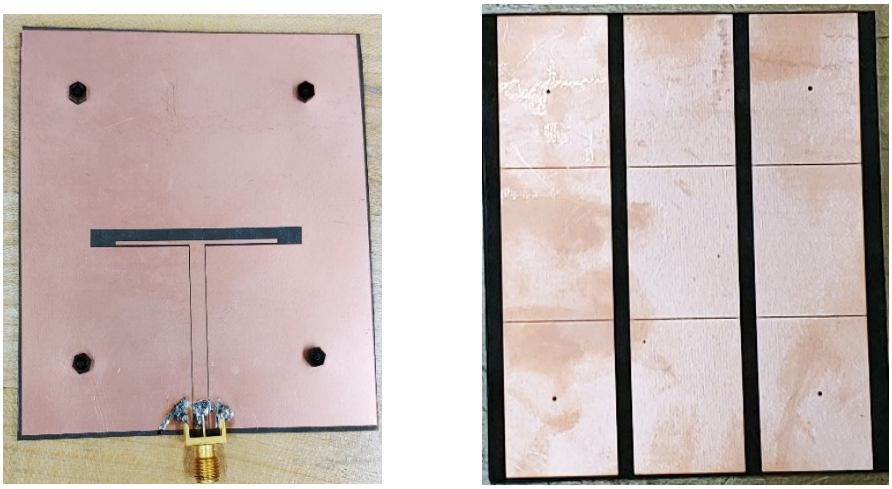

Figure 2-29: Fabricated Slotted Dipole Antenna and Rectangular Patch AMC

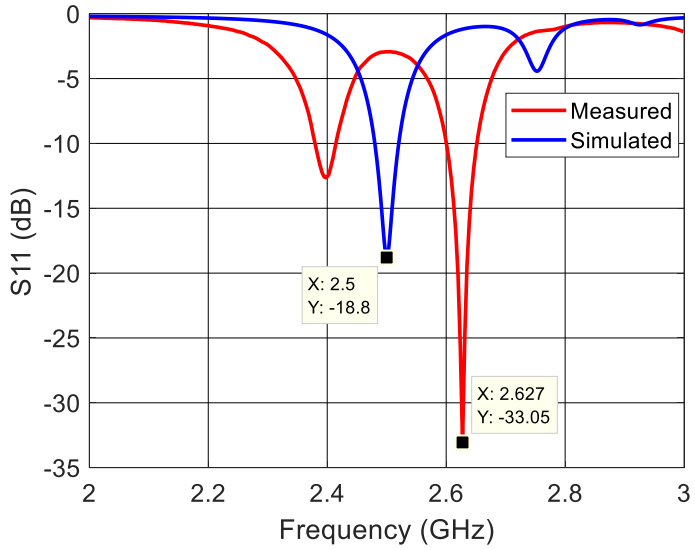

Figure 2-30: Slotted Dipole Antenna with AMC Measured and Simulated Return Loss ($Air_{gap} = 1mm$)

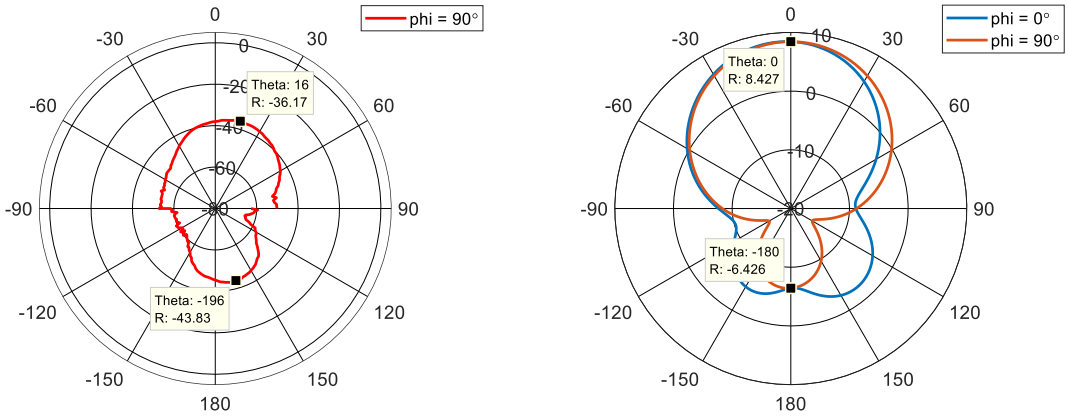

(a) (b)

Figure 2-31: Slotted Dipole Antenna with AMC Radiation Pattern:
(a) Measured (dBm); (b) Simulated

The previous figures show that the fabricated antenna and AMC layer do not function quite as designed. The resonant frequency shifts significantly to $2.627GHz$. During fabrication, it is clear that the antenna and AMC substrates were very flexible. When assembling for the $1mm$ air gap, it was not possible to ensure consistently a $1mm$ space between the two layers. The radiation pattern shows back radiation is reduced, but not eliminated. The Anechoic Chamber equipment limited the transmit antenna power to $10dBm$, higher powered transmit antennas could make the front to back ratio more evident.

3. Inverted-F Antenna with Rectangular Patch AMC

The Slotted Dipole Antenna design was quite large to be placed on a patient's body. Another antenna is desirable for reduced size. The Inverted-F Antenna is a popular antenna used in numerous applications [23], [24], [25]. There is potential to incorporate an Inverted-F Antenna with an AMC layer for a wearable antenna. This section discusses the design of the Inverted-F Antenna and integration with an AMC Layer.

3.1. Inverted-F Antenna

The Inverted-F Antenna is designed on Rogers RT/duroid 5880 with a dielectric constant $\epsilon_r = 2.2$, $\tan\delta$ of 0.0009 and dielectric height $h = 31mils$ to have a resonant frequency of $2.5GHz$. The Antenna has critical dimensions that have direct effect on the antenna's performance. For this antenna, the distance between the feeding line and shorting line are critical for determining the resonant frequency while the size of the ground plane can adjust the return loss magnitude.

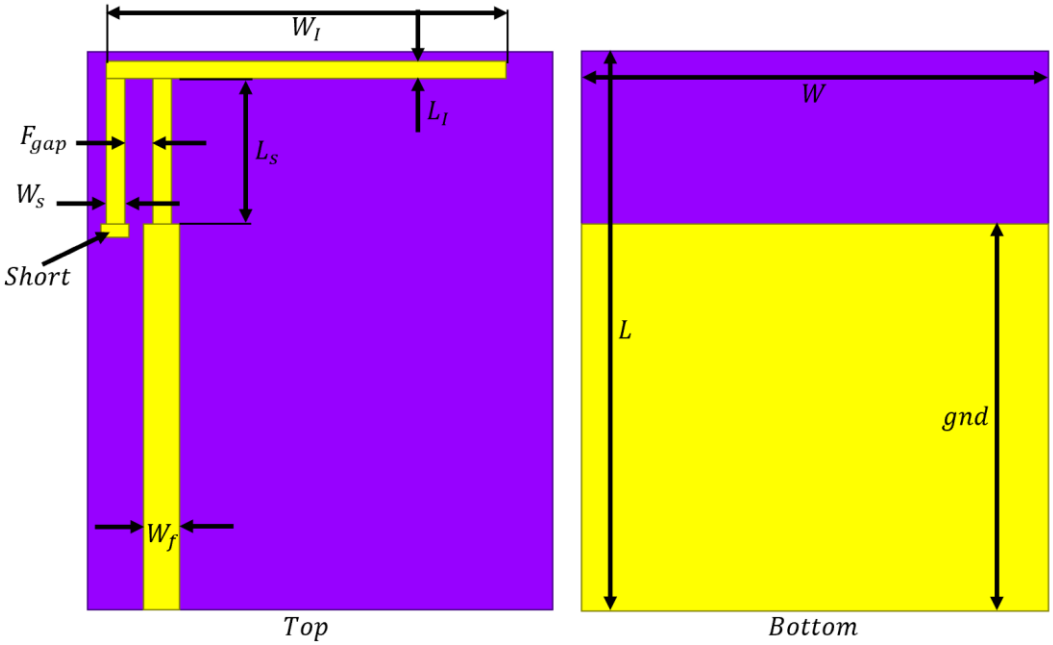

Figure 3-1: Inverted-F Antenna Model without AMC

The design of the Inverted-F Antenna was done first by using a guide for PCB Inverted-F Antennas [26]. For optimization on the desired substrate, Rogers RT/duroid 5880, two dimensions are adjusted to improve performance of the antenna. First the distance between the feeding line and the shorting line is critical for the resonant frequency of the antenna. The following plot shows the variation from the optimal dimension $F_{gap} = 1.52mm$.

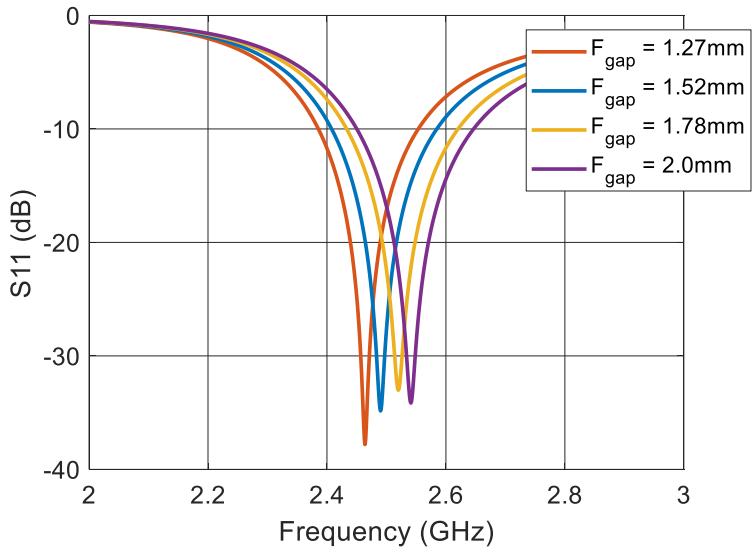

Figure 3-2: Inverted-F Antenna Variation in F_{gap} without AMC

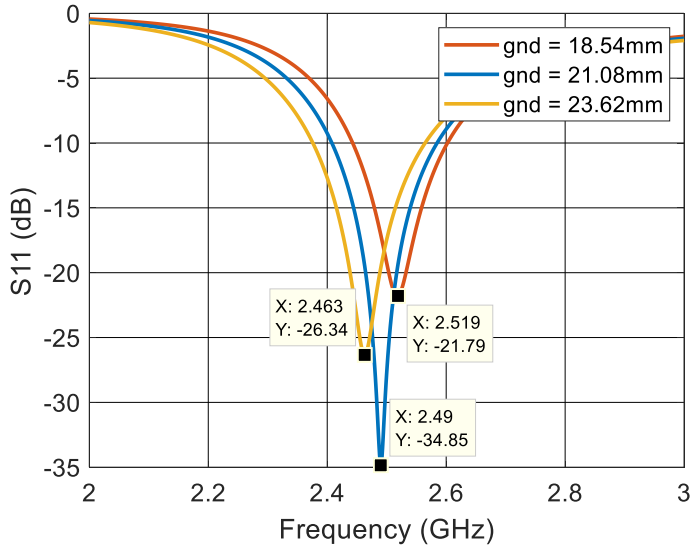

Figure 3-3:Inverted-F Antenna Variation in Ground Plane Size, gnd without AMC

Figure 3-2 shows how increasing the space between the feed line and shorting line of the Inverted-F Antenna, F_{gap}, increases the resonant frequency. In addition, the ground plane size needs to be optimized for the best return loss at the desired resonant frequency shown in Figure 3-3. The optimal dimensions for the Inverted-F Antenna are tabulated in Table 3-1. The antenna has a Return Loss of $-34.85dB$ at $2.49GHz$. The Radiation Pattern is seen in Figure 3-5.

Table 3-1: Inverted-F Antenna Optimal Dimensions

Dimension	Value
$\mathbf{F_{gap}}$	$1.52mm$
$\boldsymbol{W_f}$	$2mm$
$\mathbf{W_s}$	$1.01mm$
$\mathbf{L_s}$	$7.9mm$
$\boldsymbol{L_I}$	$0.99mm$
$\boldsymbol{W_I}$	$21.84mm$
$\boldsymbol{L}$	$30.5mm$
$\boldsymbol{W}$	$25.4mm$
$\boldsymbol{gnd}$	$21.1mm$

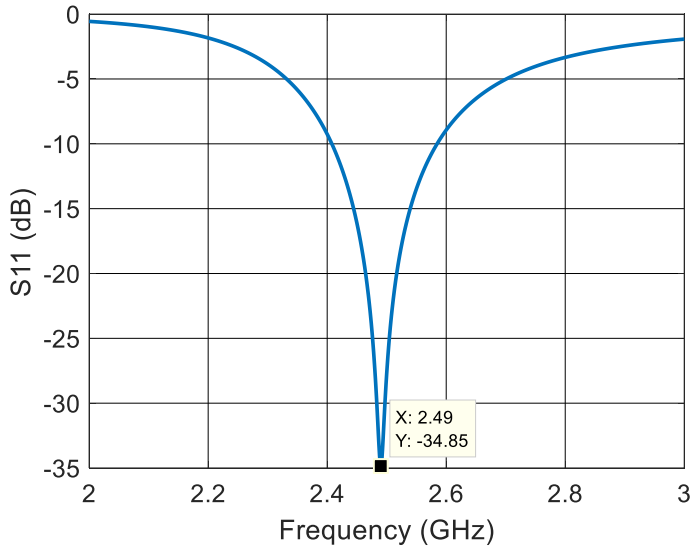

Figure 3-4: Inverted-F Antenna Return Loss without AMC on Rogers RT/duroid 5880

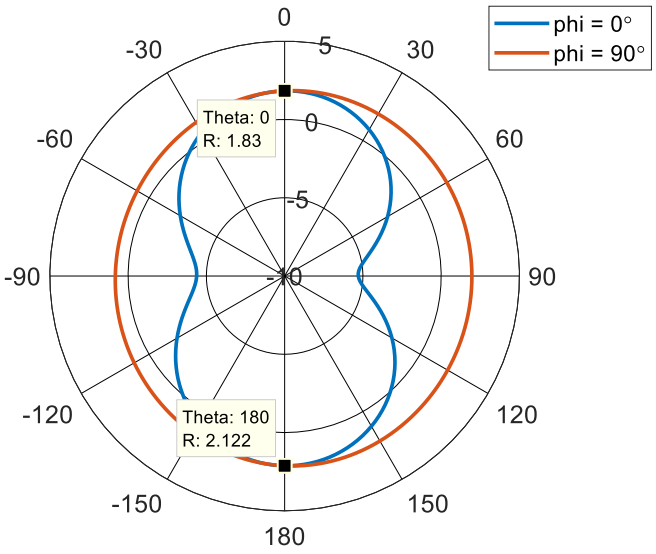

Figure 3-5: Radiation Pattern of Inverted-F Antenna without AMC on Rogers RT/duroid 5880

The Inverted-F Antenna also radiates in multiple directions; therefore, an AMC layer is desired to reduce the back radiation similar to the Slotted Dipole Antenna in Section 2. The gain of the Inverted-F Antenna is much lower than the Slotted Dipole Antenna at around $2dB$. However, this antenna is much smaller, which makes it desirable for on-body applications.

3.2. Inverted-F Antenna and Rectangular Patch AMC Integration

To prevent the backward radiation from the Inverted-F Antenna, the antenna is backed by the Rectangular Patch AMC from Section 2.3. Rather than including an air gap, a layer between the Antenna and AMC is replaced with the dielectric Rogers RT/duroid 5880. This allows for all layers of the Antenna to be put together rather than having an air gap which is difficult to physically realize. Once the combination is put together in HFSS, the optimal positioning of the Inverted-F Antenna and AMC is determined.

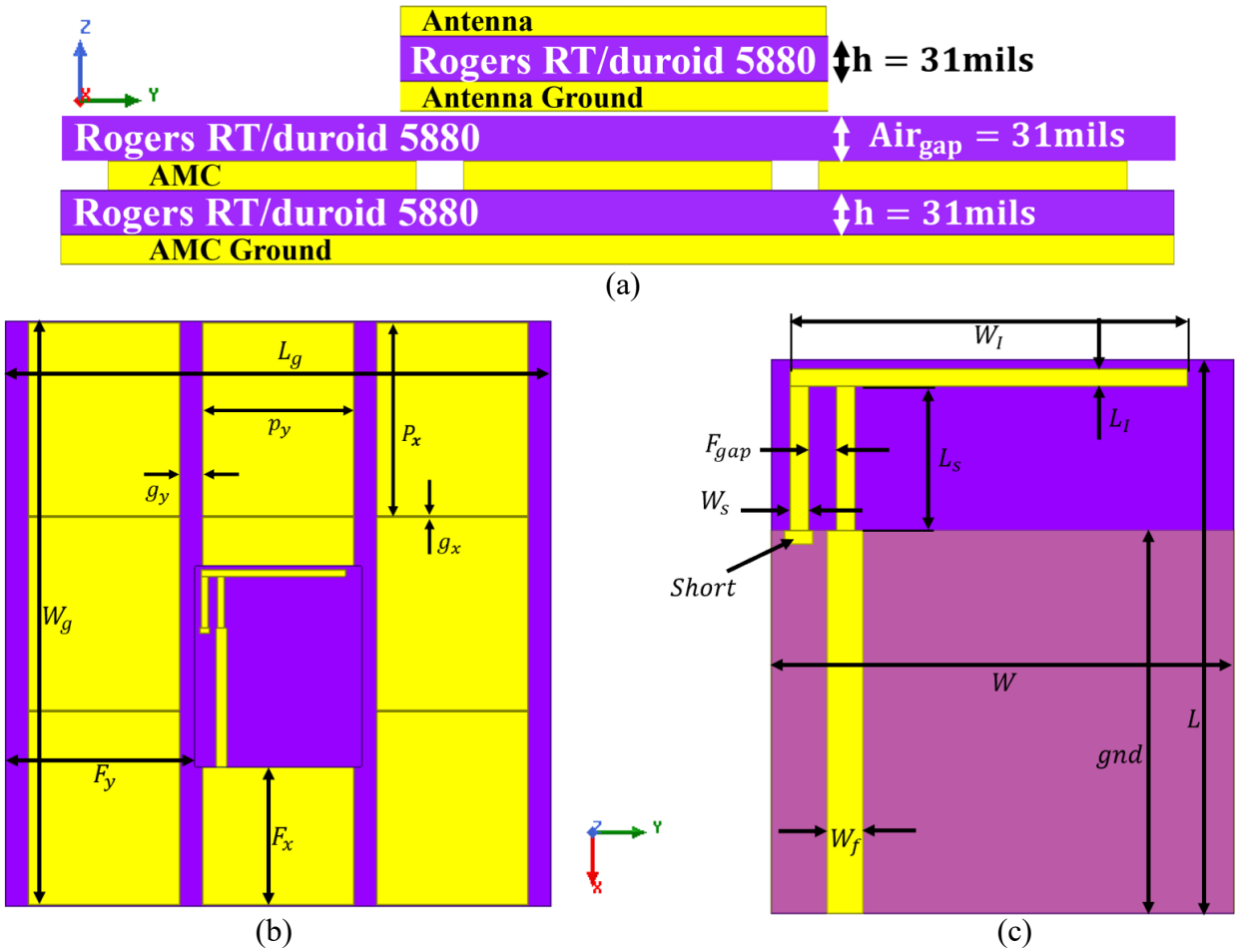

Figure 3-6: Optimal Inverted-F Antenna with Rectangular Patch AMC Placement Model: (a) Cross-Section View; (b) Top View of Inverted-F Antenna Placement on AMC (c) Inverted-F Antenna

The Rectangular Patch AMC is used with the Inverted-F Antenna to block backward radiation and improve forward gain. The optimal positioning needs to be determined similarly as the Slotted Dipole Antenna. For the Slotted Dipole, the length of the feedline is adjusted to move the radiating slot, in this case, the entire antenna is shifted along the AMC for the best position. In Figure 3-6 F_y and F_x are used to determine the location of the Inverted-F Antenna. In addition, the width of the feedline of the antenna is adjusted, W_f. The dimensions for the integration are listed in Table 3-2.

Table 3-2: Optimal Dimensions for Inverted-F Antenna and Rectangular Patch AMC Integration

Dimension	Value
$\mathbf{F_{gap}}$	$1.52mm$
$\boldsymbol{W_f}$	$1.5mm$
$\mathbf{W_s}$	$1.01mm$
$\mathbf{L_s}$	$7.9mm$
$\boldsymbol{L_I}$	$0.99mm$
$\boldsymbol{W_I}$	$21.84mm$
$\boldsymbol{L}$	$30.5mm$
$\boldsymbol{W}$	$25.4mm$
$\boldsymbol{gnd}$	$21.1mm$
$\boldsymbol{W_g}$	$89mm$
$\boldsymbol{L_g}$	$83mm$
$\boldsymbol{g_x}$	$0.2mm$
$\boldsymbol{g_y}$	$3.5mm$
$\boldsymbol{P_x}$	$29.4mm$
$\boldsymbol{P_y}$	$23mm$
$\boldsymbol{F_x}$	$21.26mm$
$\boldsymbol{F_y}$	$28.8mm$

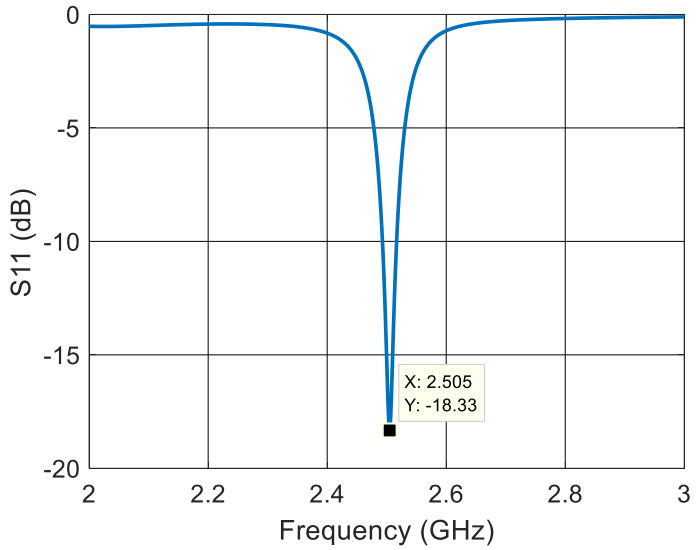

Figure 3-7: Return Loss of Inverted-F Antenna with AMC on Rogers RT/duroid 5880

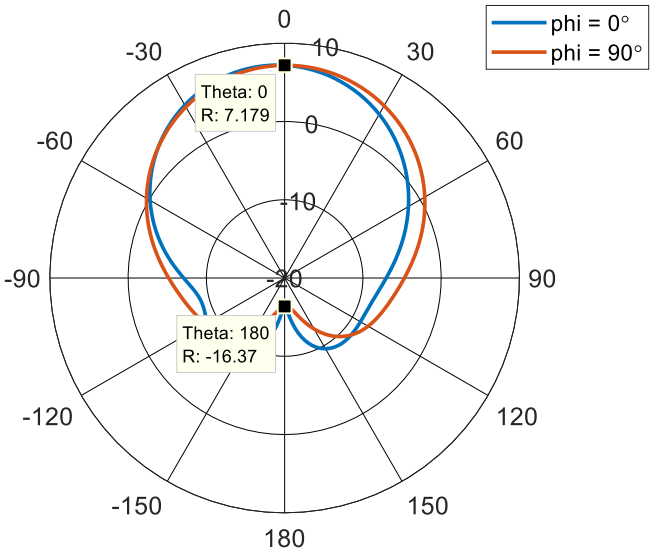

Figure 3-8: Radiation Pattern of Inverted-F Antenna with AMC on Rogers RT/duroid 5880

With the Rectangular Patch AMC, the Return Loss for the Antenna and AMC configuration is $-18.33dB$. The previous figure has the radiation pattern of the Inverted-F Antenna with the Rectangular Patch AMC. This configuration has forward gain of $7.179dB$ and a front to back ratio of $23.55dB$. Additionally, the worst-case front to back ratio is $15.34dB$. In both cases, the front to back ratios for this configuration are greater than the Slotted Dipole with AMC configurations.

Table 3-3: Slotted Dipole Antenna and Inverted-F Antenna Simulation Results with and without AMC

	Slotted Dipole (No AMC)	**Inverted-F (No AMC)**	**Slotted Dipole (With AMC) $Air_{gap} = 1mm$**	**Inverted-F (With AMC)**
Overall Height	$31mils$	$31mils$	$2.58mm$	$2.36mm$
$f_{resonance}$	$2.505GHz$	$2.49GHz$	$2.5GHz$	$2.5GHz$
Return Loss	$-26.95dB$	$-34.85dB$	$-18.8dB$	$-18.33dB$
Forward Gain	$5.2dB$	$1.8dB$	$8.427dB$	$7.17dB$
Front to Back Ratio	–	–	$14.85dB$	$23.55dB$
Worst-Case Front to Back Ratio	–	–	$10.89dB$	$15.34dB$

Both the Slotted Dipole and Inverted-F Antenna are backed with the Rectangular Patch AMC. Although the Slotted Dipole Antenna by itself has a higher forward gain than the Inverted-F Antenna at $5.2dB$, when backed with the AMC, both antennas have very comparable forward gains. The Inverted-F Antenna with the AMC layer has the largest front to back ratio of $23.55dB$. Along with the largest worst-case front to back ratio of $15.34dB$. In addition, that configuration has the smallest overall height of $2.36mm$. The integration of the Inverted-F Antenna with the AMC shows the greatest performance in terms of front to back ratio and overall height making it a good choice for off-body communication in Wireless Medical Telemetry systems.

3.3. Inverted-F Antenna with Human Body Model without Rectangular Patch AMC

Similar to Section 2.6, the Inverted-F Antenna is simulated with the Human Arm Model without the Rectangular Patch AMC to show the effects of the dielectric load caused by the human tissue. The model for the simulation is shown in the next figure. The Antenna is approximately $2mm$ above the human tissue.

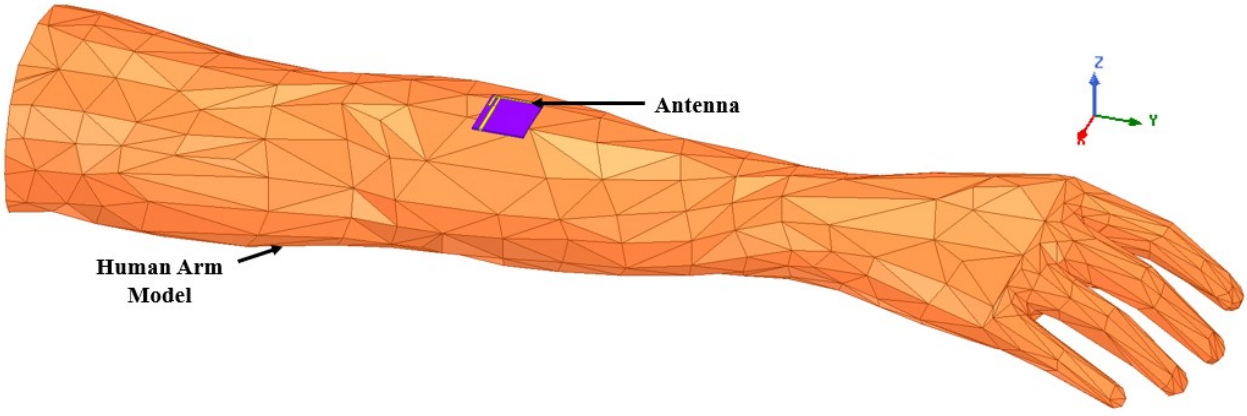

Figure 3-9: HFSS Model of Inverted-F Antenna without AMC Above Human Arm

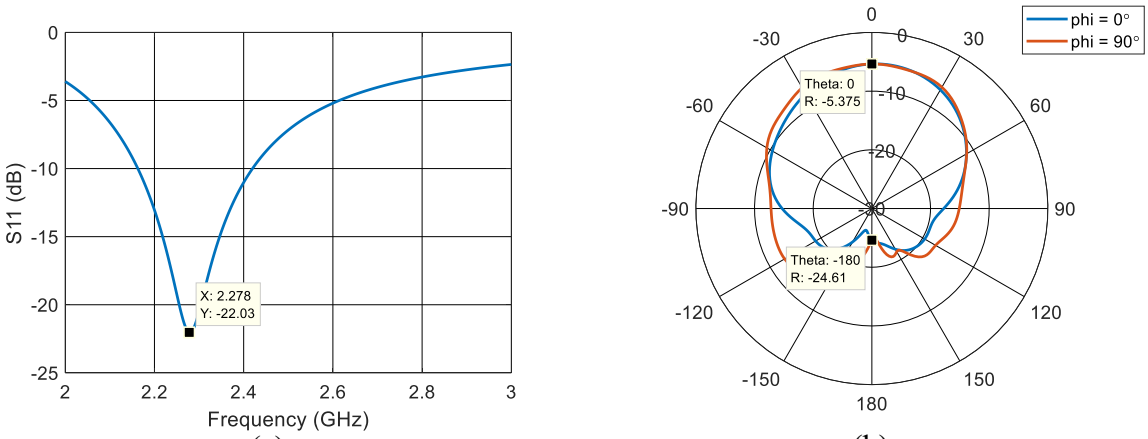

(a) (b)

Figure 3-10: Inverted-F Antenna without AMC Placed Above Human Arm: (a) Return Loss; (b) Radiation Pattern

The Inverted-F Antenna has a shift in resonant frequency to $2.278GHz$ but still a good Return Loss of $-22dB$. Compared to the Slotted Dipole Antenna when the Human Arm Model is introduced, the return loss is still very good, even at the wrong frequency for the Inverted-F Antenna. The radiation pattern changes significantly due to the dielectric load in Figure 3-10. The Inverted-F Antenna has been used alone for on-body applications seen in [5]; it makes sense that tuning this antenna for the on-body application is feasible.

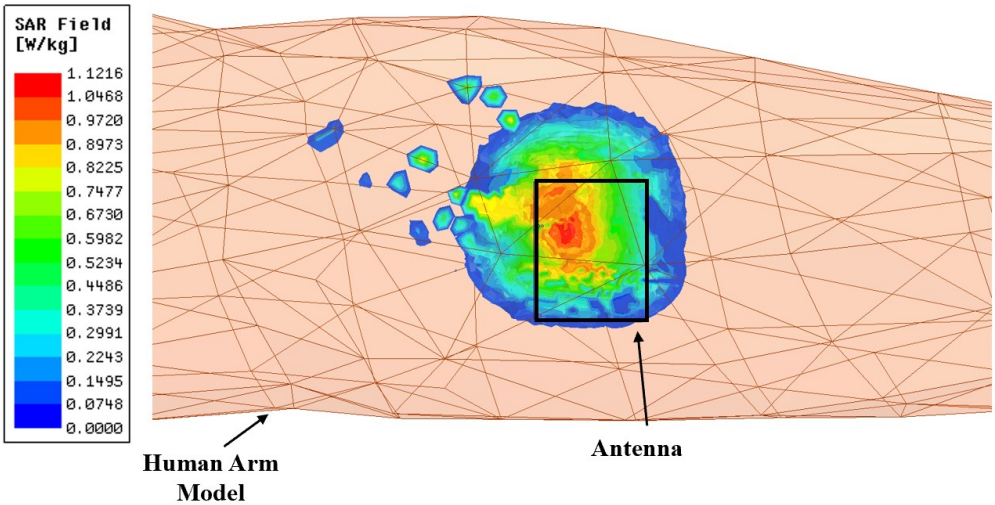

Figure 3-11: Average SAR Simulation of Inverted-F Antenna without AMC (Input Power: $10mW$)

Without the AMC Layer, the Arm Model has a max SAR level of $1.12\ W/kg$. Although this is below the limits set by the FCC, the addition of the Rectangular Patch AMC in the next section should significantly reduce the backward radiation toward the human body, lowering SAR levels further.

3.4. Inverted-F Antenna with Human Body Model with Rectangular Patch AMC

The Artificial Magnetic Conductor should reduce the effects of the dielectric load caused by the human tissue as seen with the Slotted Dipole Antenna in Section 2.7. Here, the Rectangular Patch AMC is introduced to the model with the Inverted-F Antenna to improve the on-body antenna performance. The Antenna and AMC configuration is the same as in Section 3.2, Figure 3-6, and Table 3-2.

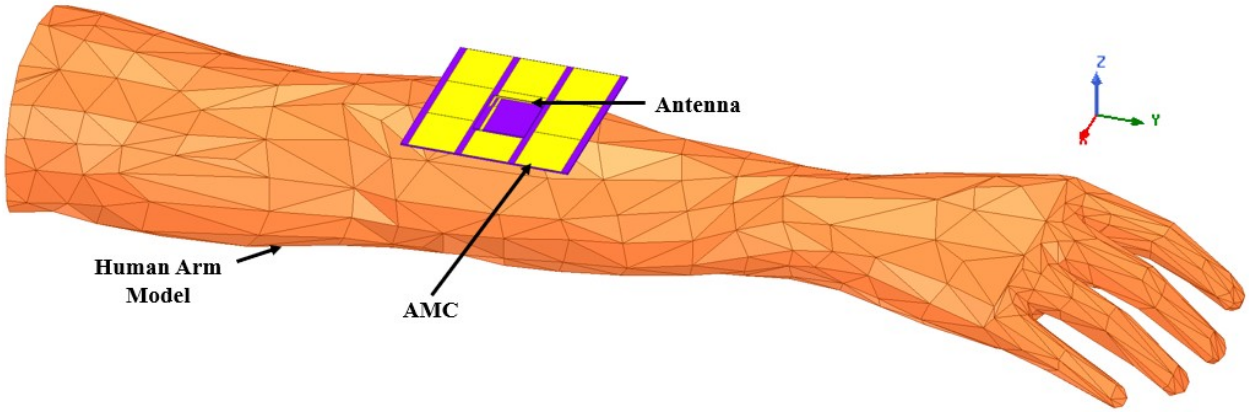

Figure 3-12: HFSS Model of Inverted-F Antenna with AMC Above Human Arm

With the addition of the Rectangular Patch AMC, the effects of the Human Arm Model are minimal. The Return loss is now $-17.9dB$ from $-18.3dB$ with a slight frequency shift to $2.508GHz$. The forward gain remains almost constant at $7.2dB$. In Figure 3-14, the average SAR levels are modeled using HFSS when the AMC is added.

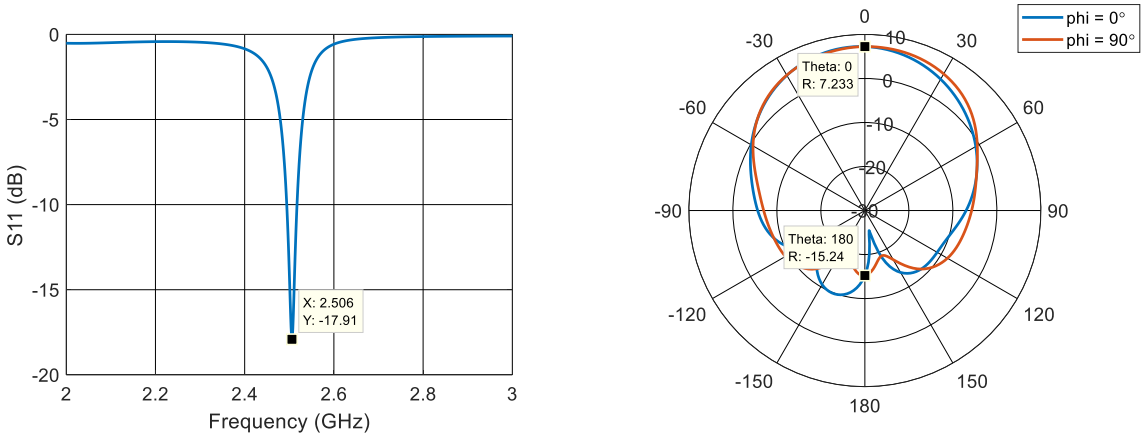

(a) (b)

Figure 3-13: Inverted-F Antenna with AMC Placed Above Human Arm: (a) Return Loss; (b) Radiation Pattern

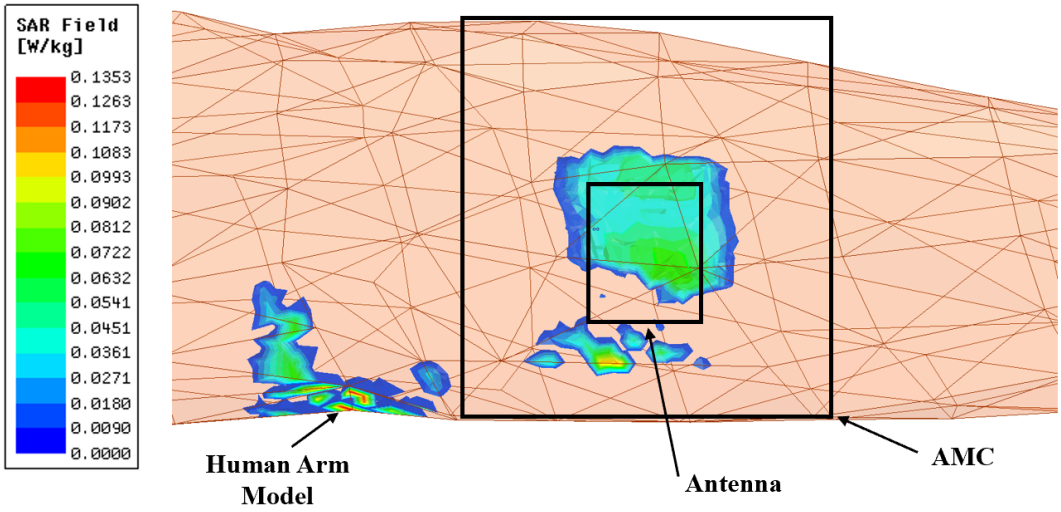

Figure 3-14: Average SAR Simulation of Inverted-F Antenna with AMC (Input Power: $10mW$)

The AMC reduces the backward radiation directly behind the antenna significantly from over $1.1\,W/kg$ to around $0.08\,W/kg$. The Inverted-F Antenna and AMC configuration can also be used for on-body applications. The AMC layer reduces backward radiation, preventing radiation from entering a person's body as well as prevent the large dielectric load of the body affecting the performance of the antenna.

Table 3-4: Inverted-F Antenna on Arm Simulation Results

	Free Space with AMC	**Arm no AMC**	**Arm with AMC**
$f_{resonance}$	$2.505GHz$	$2.278GHz$	$2.506GHz$
Return Loss	$-18.33dB$	$-22.03dB$	$-17.91dB$
Forward Gain	$7.179dB$	$-5.375dB$	$7.23dB$
SAR	$-$	$1.1216\ W/kg$	$0.08\ W/kg$
	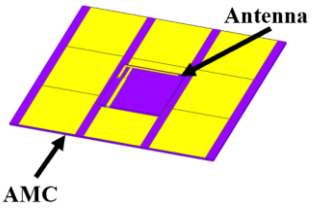	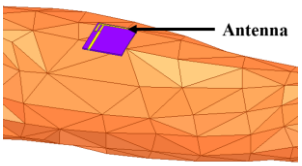	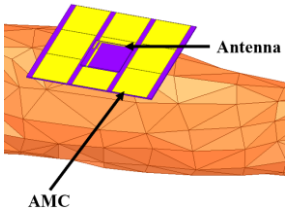

The Artificial Magnetic Conductor layer significantly reduced the back radiation and prevents the Human Arm Model from altering the performance of the Inverted-F Antenna. Similar results were seen with the Slotted Dipole Antenna in Table 2-4 when it was integrated with the AMC and placed on the Human Arm Model. In this case, the Inverted-F Antenna shows promise for being tuned without the AMC for on-body applications with good return loss but only a shift in frequency to $2.278GHz$. With the AMC layer, additional tuning is not required as the resonant frequency stays at $2.506GHz$ with a return loss of $-17.91dB$ shown in Table 3-4. The AMC reduces the SAR levels dramatically from $1.12\ W/kg$ without the AMC layer to $0.08\ W/kg$ with the AMC layer with input power of $10mW$ but are still FCC SAR limits.

3.5. Experimental Validation

The Inverted-F Antenna is fabricated on Rogers RT/duroid 5880 ($\epsilon_r = 2.2$, $\tan\delta$ of 0.0009 and dielectric height $h = 31mils$). The Inverted-F Antenna dimensions are in Table 3-2. The results of the experimental measurements are shown in this section.

3.5.1. Measured Inverted-F Antenna

The Inverted-F Antenna is tested using the network analyzer. Due to power limitations in the Anechoic Chamber, the radiation pattern was not able to be measured. However, the results from the Network Analyzer are shown in Figure 3-16.

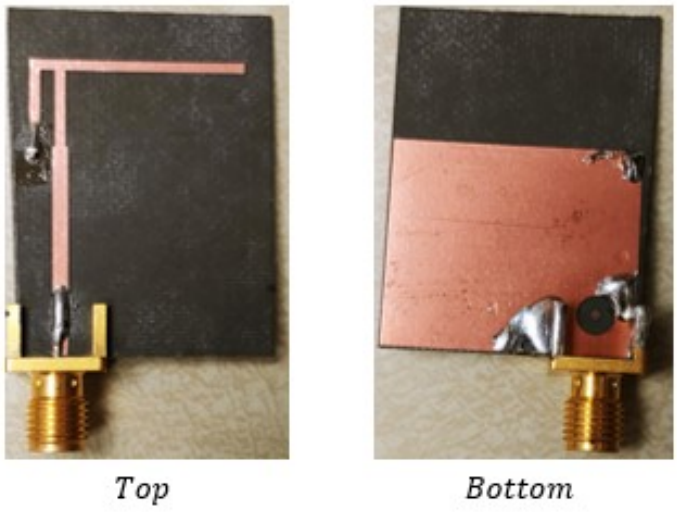

Figure 3-15: Fabricated Inverted-F Antenna

The fabricated antenna has a low return loss at $-17.21dB$, but only shifts slightly in frequency to $2.474GHz$ from the designed $2.5GHz$. As mentioned earlier, the radiation pattern could not be attained due to power limitations of the transmit antenna in the Anechoic Chamber. In the next section, the antenna is integrated with the Rectangular Patch AMC and the Inverted-F Antennas functionality is proven.

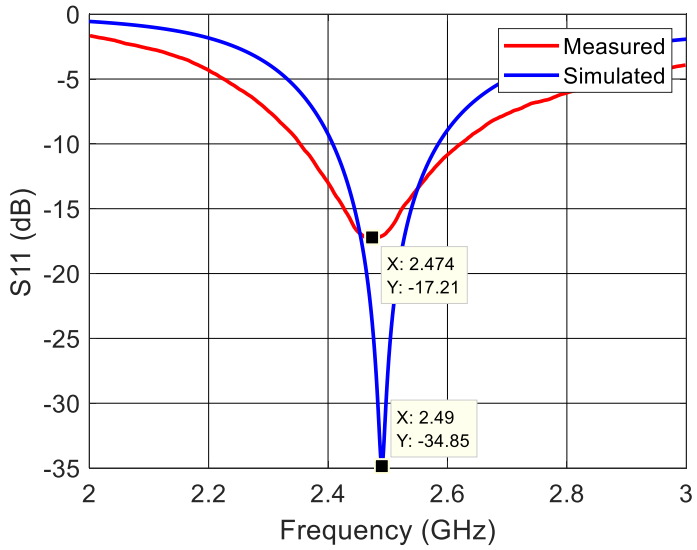

Figure 3-16: Measured and Simulated Return Loss of Inverted-F Antenna

3.5.2. Measured Inverted-F Antenna and Rectangular Patch AMC

The Rectangular Patch AMC is integrated with the Inverted-F Antenna. Simulations originally required a layer of substrate between the Antenna and AMC. In addition, a bottom feed connector was required to go through the AMC Layer. Although functioning in simulation, fabrication proved to be difficult. Because of the very low profile, a side fed connector could not be used with the thin layer of dielectric spacing. In addition, with the bottom fed connector through the AMC layer, it was not possible to adjust the antenna to find the best location for electrical coupling. Instead, to prove the functionality of the antenna and AMC, a side fed connector is attached and a layer of Styrofoam is used to suspend the antenna above the AMC. The setup is shown in Figure 3-17.

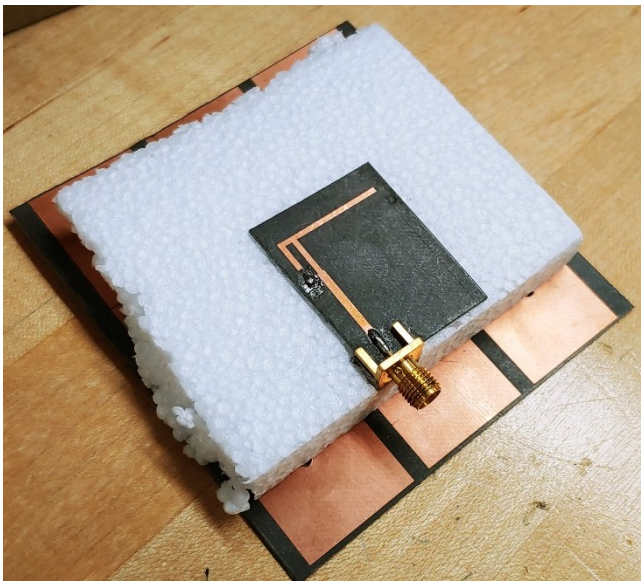

Figure 3-17: Inverted-F Antenna Above Rectangular Patch AMC

The setup has a piece of Styrofoam with a height of $12mm$. The HP8753ET Network Analyzer is used to measure the setup's resonant frequency and return loss in Figure 3-18.

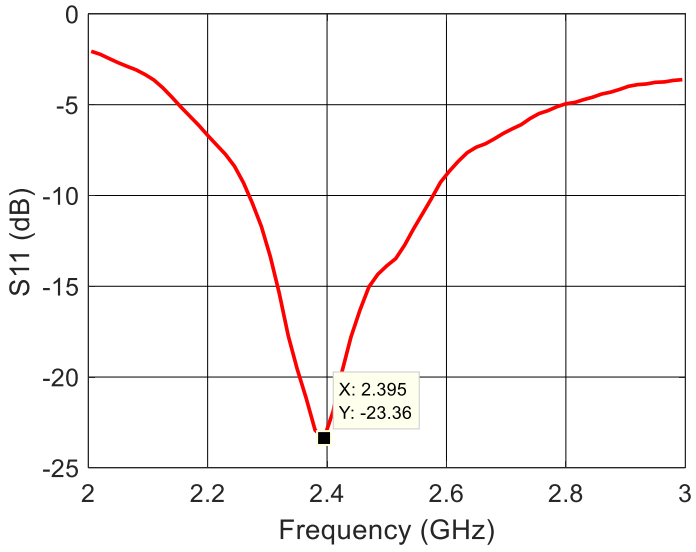

Figure 3-18: Measured Return Loss of Inverted-F Antenna Above AMC

The Anechoic Chamber is used to measure the radiation pattern of the Inverted-F Antenna with the Rectangular Patch AMC. The configuration shown in Figure 3-17 is used for the measurements. These measurements show that the Inverted-F Antenna is radiating which was not captured in the previous section.

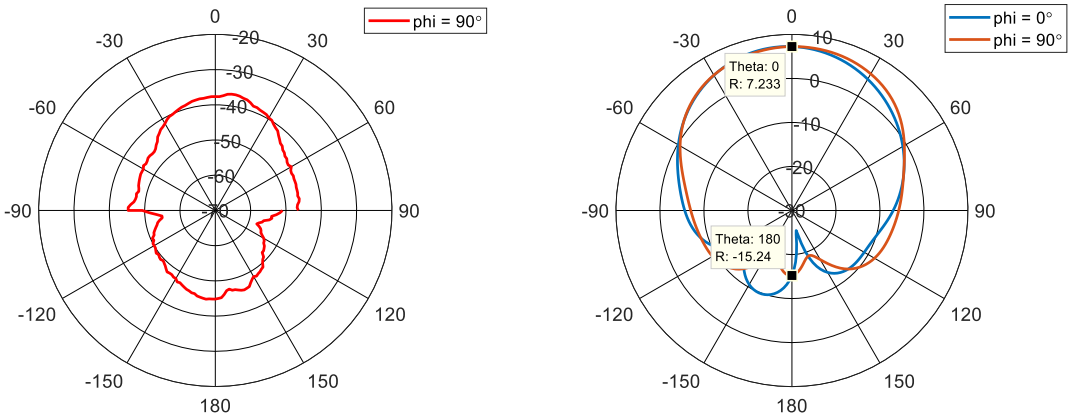

(a) (b)

Figure 3-19: Inverted-F Antenna with AMC Radiation Pattern:
(a) Measured (dBm); (b) Simulated

The Measured Return Loss is good at $-23.36dB$ with a shift in resonant frequency to $2.395GHz$. The measured radiation pattern in the previous figure shows that the back radiation is blocked but not eliminated. This could be due to the power limitation in the anechoic chamber, increased power may show the bigger different in absorbed power for the front and back of the antenna. Additionally, a hole was already drilled for a bottom fed connector which could allow some back radiation. Further work is required to determine a better way to assemble the antenna combination as shown in the simulations.

4. Square Slotted AMC

The Rectangular Patch AMC has a large unit cell. In order to have a functioning AMC layer, an array of unit cells is required. If the unit cell size were reduced, the overall AMC layer could be minimized. A smaller AMC cell, the Square Slotted AMC unit cell is found in the literature [20]. This AMC has an area of 1 square centimeter, much smaller than the Rectangular Patch. Therefore, an array of Square Slotted unit cells could create a smaller overall AMC layer. This AMC is designed on Rogers RT/duroid 6010LM which has a dielectric constant $\epsilon_r = 10.2$, loss tangent $\delta = 0.0023$ and height $h = 1.52mm$. A disadvantage of this substrate is that it is not flexible, unlike the substrates in the previous sections. Therefore, this AMC layer must be rigid.

4.1. Square Slotted Artificial Magnetic Conductor

The reduced size Artificial Magnetic Conductor uses a smaller unit cell size that is 1 square centimeter, much smaller than the Rectangular Patch AMC from section 2.3. The new AMC is on Rogers RT/duroid 6010LM, ($\epsilon_r = 10.2$, $\delta = 0.0023$ and $h = 1.27mm$). This unit cell was originally designed for dual frequency applications in [20]. However, in this application, only the reduced size is desired. In Figure 4-1 the diagram of the Slotted Square Artificial Magnetic Conductor unit cell is visible.

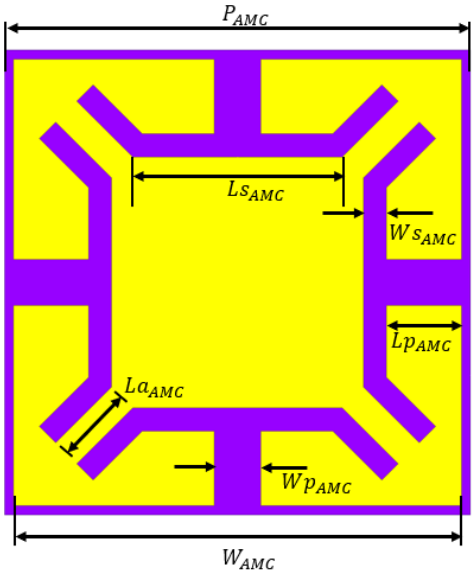

Figure 4-1: HFSS Model Square Slotted AMC Unit Cell

The dimensions of the unit cell above are tuned for a 0 degree phase difference at $2.5GHz$. The Unit Cell 0 degree reflection frequency can be easily adjusted by changing some critical dimensions. Below, the dimensions Ls_{AMC} and La_{AMC} are varied to show the shifting optimal frequencies.

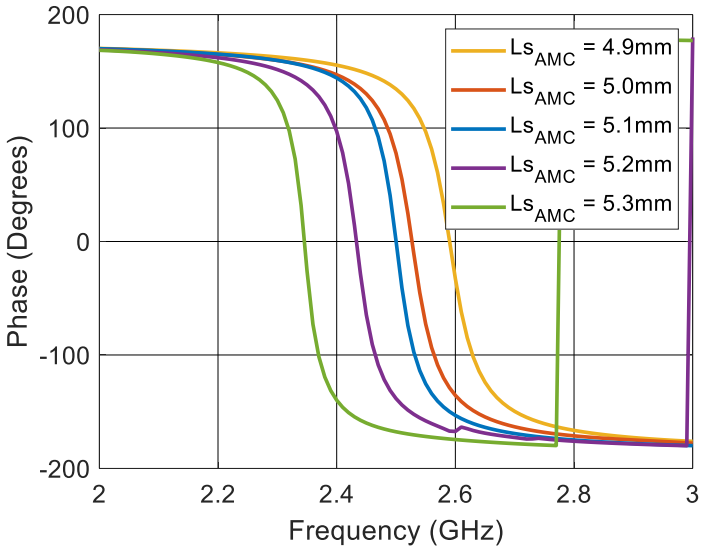

Figure 4-2: Phase Plot of Square Slotted AMC Unit Cell Varying Ls_{AMC}

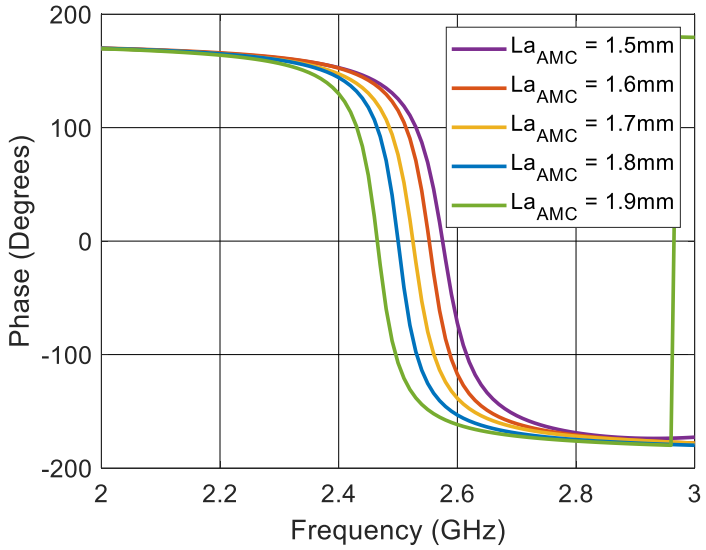

Figure 4-3:Phase Plot of Square Slotted AMC Unit Cell Varying La_{AMC}

Table 4-1: Optimal Dimensions for Square Slotted Unit Cell on Rogers RT/duroid 6010LM

Dimension	Value
$\mathbf{P}_{AMC}$	$10mm$
W_{AMC}	$9.6mm$
$\mathbf{Ls}_{\mathbf{AMC}}$	$5.1mm$
La_{AMC}	$1.8mm$
$\mathbf{Lp}_{\mathbf{AMC}}$	$1.6mm$
$\mathbf{Ws}_{\mathbf{AMC}}$	$0.5mm$
Wp_{AMC}	$1.0mm$

The previous figures show how small changes in dimensions of the Unit Cell can adjust the design frequency. The other dimensions can also be adjusted for shifts in optimal frequency. In this design, $2.5GHz$ is desired. The dimensions in Table 4-1 are the optimal dimensions of the Square Slotted AMC unit cell for the desired frequency. Figure 4-4 contains the phase plot of the unit cell with the optimal dimensions.

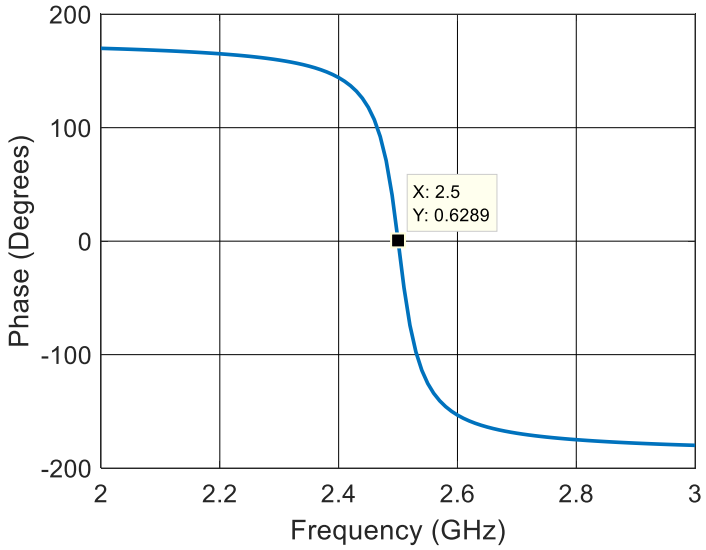

Figure 4-4: Phase Plot of Optimized Square Slotted AMC Unit Cell on Rogers RT/duroid 6010LM

Using the Square Slotted unit cell, a new AMC layer could be created. Because each individual cell is smaller than the first Rectangular Patch AMC, the total AMC can be miniaturized. This can potentially allow for a smaller overall antenna and AMC configuration, which is preferable for on-body applications. However, the rigidness of the substrate needs to be considered when talking about the advantages or challenges of this design.

5. Conclusion

The designed antennas with AMC configurations are shown to block backward radiation while improving the forward gain of the antenna. The Slotted Dipole Antenna alone has forward gain of $5.2dB$, with the inclusion of the AMC layer, the gain increases to $8.427dB$ when $Air_{gap} = 1mm$. The Inverted-F Antenna alone has forward gain around $2dB$, but when the AMC layer is included the forward gain increases dramatically to $7.17dB$, results in Table 3-3. The front to back ratio is significantly improved with the Inverted-F Antenna with the AMC layer, to $23.55dB$, including the largest worst-case front to back ratio of $15.34dB$.

The Slotted Dipole Antenna with AMC is shown to be flexible in Section 2.5 and Table 2-3 with $Air_{gap} = 6mm$. The Antenna and AMC configuration without a flexible substrate has the highest forward gain of $7.486dB$. However, the Convex and Concave curvatures have only slightly lower forward gain of $7.11dB$ and $7.08dB$ respectively. The shifts in resonant frequency are negligible. Additionally, front to back ratios are comparable to the flat antenna configuration. Reducing the size of the air gap could improve the performance of the curved configurations as it did with the flat antenna and AMC configuration.

SAR simulations of the antennas with and without the AMC layer are performed in HFSS. When the Slotted Dipole Antenna is introduced to the Human Arm Model, a large frequency shift to $3.071GHz$ is obtained with poor return loss of $-6.39dB$. Once the AMC layer is included, the antenna performance is near ideal with good forward gain of $7.623dB$. The SAR experienced by the arm reduced from $0.244\,W/kg$ to $0.028\,W/kg$ when the AMC layer is introduced. The Inverted-F Antenna however had good return loss when the arm was introduced with the AMC layer of $-22.03dB$ but a resonant frequency shift to $2.278GHz$. The antenna can most likely be tuned back to the desired resonant frequency in this configuration. However, with input power of

$10mW$, the SAR level obtained, $1.1216\ W/kg$, reached near the limit imposed by the FCC of $1.6\ W/kg$. When the AMC layer is introduced, further tuning of the antenna is not required while the desired resonant frequency is returns, $2.506GHz$, and the SAR directly behind the antenna reduces to about $0.08\ W/kg$.

The Antennas and AMC are fabricated on Rogers RT/duroid 5880, ($\epsilon_r = 2.2, \tan\delta = 0.0009$ and $h = 31mils$). Alone the Slotted Dipole Antenna functions as designed with a slight shift of resonant frequency to $2.485GHz$ with good return loss of $-34.53dB$. The Slotted Dipole Antenna with the AMC combination was difficult to assemble with a consistent $Air_{gap} = 1mm$. The measured results show a frequency shift to $2.627GHz$ with a return loss of $-33.05dB$. The radiation pattern shows back radiation being reduce in Figure 2-31 however forward gain is not shown as enhanced. The Inverted-F Antenna was also difficult to integrate with the AMC layer. Styrofoam was used to demonstrate the AMC and antenna functionality seen in Figure 3-17. There was a frequency shift to $2.395GHz$ with a return loss of $-23.36dB$.

5.1. Future Work

The Rectangular Patch AMC is quite large at almost 81 square centimeters. A small AMC unit cell, the Square Slotted AMC cell is introduced and designed for $2.5GHz$ for potential use in a smaller AMC layer. The smaller layer could allow for the overall antenna and AMC configuration to reduce in overall size however, the substrate rogers RT/duroid 6010LM is rigid, meaning it could not be used as a flexible antenna and AMC configuration. Additional work is also necessary to improve the technique or method to combine the Antennas with the AMC layer. The integration of these layers has proven to be difficult although their overall functionality is shown.

References

[1] K. S. Nikita, Handbook of Biomedical Telemetry, Hoboken, New Jersey: John Wiley & Sons, Inc., 2014.

[2] Autosport Labs, "RaceCapture/Pro 3," 2016. [Online]. Available: https://www.autosportlabs.com/wp-content/uploads/2018/08/RaceCapture_Pro-MK3-product-brief.pdf.

[3] J. Spacey, "11 Examples of Telemetry," 03 December 2016. [Online]. Available: https://simplicable.com/new/telemetry.

[4] L. Shu, Y. Yu, W. Chen, H. Hua, Q. Li, J. Jin and X. Xu, "Wearable Emotion Recognition Using Heart Rate Data from a Smart Bracelet," *Sensors (Basel, Switzerland),* vol. 20, p. 718, 2020.

[5] G. Wolgast, C. Ehrenborg, A. Israelsson, J. Helander, E. Johansson and H. Manefjord, "Wireless Body Area Netowrk for Heart Attack Detection [Education Corner]," *IEEE Antennas and Propagation Magazine,* vol. 58, no. 5, pp. 84-92, 2016.

[6] Welch Allyn, "TAGECG® WEARABLE ECG SENSOR," Welch Allyn, 2018. [Online]. Available: https://www.welchallyn.com/en/products/categories/cardiopulmonary/wearable-ecg-monitors/tagecg-wearable-ecg-sensor.html.

[7] Dexcom, Inc., "Dexcom Continuous Glucose Monitoring," 2020. [Online]. Available: https://www.dexcom.com/.

[8] X.-F. Teng, Y.-T. Zhang, C. C. Y. Poon and P. Bonato, "Wearable Medical Systems for p-Health," *IEEE Reviews in Biomedical Engineering,* vol. 1, pp. 62-74, 2008.

[9] S. Movassaghi, M. Abolhasan, J. Lipman, D. Smith and A. Jamalipour, "Wireless Body Area Networks: A Survey," *IEEE Communications Surveys & Tutorials,* vol. 16, pp. 1658-1686, 2014.

[10] M. Salayma, A. Al-Dubai, I. Romdhani and Y. Nasser, "Wireless Body Area Network (WBAN): A Survey on Reliability, Fault Tolerance, and Technologies Coexistence," *ACM Computing Surveys,* vol. 50, no. 1, pp. 1-38, 2017.

[11] Federal Communications Commission, "FCC Online Table of Frequency Allocations," 6 March 2020. [Online]. Available: https://transition.fcc.gov/oet/spectrum/table/fcctable.pdf.

[12] C. Gabriel, S. Gabriel and E. Corthout, "The dielectric properties of biological tissues: I. Literature Survey," *Physics in Medicine and Biology,* vol. 41, no. 11, pp. 2231-2249, 1996.

[13] S. Gabriel, S. Lau and C. Gabriel, "The dielectric properties of biological tissues: II. Measurements in the frequency range 10 Hz to 20GHz," *Physics in Medicine and Biology,* vol. 41, no. 11, pp. 2251-2269, 1996.

[14] D. A. Sanchez-Hernandez, High Frequency Electromagnetic Dosimetry, 2009.

[15] R. F. Cleveland Jr., "Compliance with FCC Exposure Guidelines for Radiofrequency Electromagnetic Fields," 2004.

[16] K. Chan, *Overview of RF Exposure Concepts and Requirements,* Federal Communications Commission, 2005.

[17] M. Iyer, *Compact Antenna with Artificial Magnetic Conductor for Noninvasive Continuous Blood Glucose Monitoring,* 2018.

[18] G. A. Conway and W. G. Scanlon, "Antennas for Over-Body-Surface Communication at 2.45 GHz," *IEEE Transactions on Antennas and Propagation,* vol. 57, no. 4, pp. 844-855, 2009.

[19] M. Hosseinipanah and Q. Wu, "Equivalent Circuit Model for Designing of Jerusalem Cross-Based Artificial Magnetic Conductors," *Radioengineering,* vol. 18, no. 4, pp. 544-550, 2009.

[20] S. X. Ta and I. Park, "Design of Miniaturized Dual-Band Artificial Magnetic Conductor with Easy Control of Second/First Resonant Frequency Ratio," *Journal of Electromagnetic Engineering and Science,* vol. 13, no. 2, pp. 104-112, 2013.

[21] S. M. Saeed, C. A. Balanis, C. R. Birtcher, A. C. Durgun and H. N. Shaman, "Wearable Flexible Reconfigurable Antenna Integrated With Artificial Magnetic Condcutor," *IEEE Antennas and Wireless Propagation Letters,* vol. 16, pp. 2396-2399, 2017.

[22] C. A. B. C. R. B. Saud M. Saeed, "Inkjet=Printed Flexible Reconfigurable Antenna for Conformal WLAN/WiMAX Wireless Devices," *IEEE Antennas and Wireless Propagation Letters,* vol. 15, pp. 1979-1982, 2016.

[23] T. Houret, L. Lizzi, F. Ferrero, C. Danchesi and S. Boudaud, "DTC-Enabled Frequency-Tunable Inverted-F Antenna for IoT Applications," *IEEE Antennas and Wireless Propagation Letters,* vol. 19, no. 2, pp. 307-311, 2020.

[24] Q.-H. Wu, X.-W. Xuan, W. Wang, K. Li and H.-B. Zhao, "A miniaturized implantable planar inverted-F antenna for biotelemetry applications at 2.45 GHz industrial, scientific, and medical band," *Microwave and Optical Technology Letters,* vol. 62, no. 1, pp. 391-396, 2020.

[25] S. Soghi, S. H. M. Armaki and M. Fartookzadeh, "Miniaturized dual-band PCB inverted F/L antenna for nano-satellite application," *Microwave and Optical Technology Letters,* vol. 59, no. 11, pp. 2898-2903, 2017.

[26] S. Labs, *AN1088: Designing with an Inverted-F 2.4GHz PCB Antenna.*